FIBROUS MODEL FOR THE SIMULATION OF THE CYCLIC BEHAVIOUR OF 3D REINFORCED CONCRETE FRAMES

Rajendra Kumar Varma, Prof. Joaquim Barros and José Sena-Cruz

Report 07-DEC/E-04

Universidade do Minho

Escola de Engenharia
Departamento de Engenharia Civil

TABLE OF CONTENTS

ABSTRACT

Non-linear finite element analysis has attracted a lot of attention in last few decades, as real life problems dealing with analysis of concrete beams and columns are generally non-linear in nature. This project deals with non-linear analysis of beam and columns, using Timoshenko beam theory. The Timoshenko beam theory is applied to every element, but before applying the theory the element is divided into fibers. The fibers as a whole will govern the behavior of element. The section of each element is divided in "finite elements". Each finite element is a fiber along the length of element. Each fiber element is independent in terms of the material constitutive laws, which govern the behavior, while at the same time they are associated to each other by the relation of displacements. The material laws of each fiber deals with the stress-strain relation

The numerical results are compared with the experimental results, which show a reasonable correlation, and in turn demonstrate the capability of the proposed model to depict the cyclic behavior of concrete elements.

ACKNOWLEDGEMENTS

INTRODUCTION

Fiber model is one of the robust techniques which can describe the non linear material behavior of element as a whole, which may contain various type of material along its longitudinal axis. The element can contain various types of materials which are characterized by different type of material constitutive laws for stress and strain. This method assumes that the element can be divided into longitudinal fibers (like steel or concrete). The implementation considered the possibility of using three types of fibers

     (i) concrete fibers,

     (ii) steel fibers and

     (iii) linear isotropic fibers.

The concrete and steel fibers are characterized by the cyclic constitutive laws proposed by Chang and Mander (1994).

The report begins primarily with basic theories and laws which are required for implementation of fiber model. The report can be broadly divided in three parts as constitutive laws, Timoshenko beam theory and implementation of fiber model. The cyclic constitutive laws for concrete and steel are described in the section-1, which is followed by the Timoshenko beam theory in section-2 and section-3 illustrates fiber model implementation with examples and conclusions.

1. CONSTITUTIVE LAWS

The section below describes the modified cyclic constitutive laws for concrete and steel derived from Chang and Mander (1994). The cyclic law described here considers the degradation also.

1.1 CONCRETE CONSTITUTIVE CYCLIC LAWS

1.1.1) Types of Curves

The behavior of concrete can be described by three basic components, namely:

a) *Envelope Curves*:

Basically these curves represent the uniaxial monotonic loading of concrete and can be considered to be the foundation for the other constitutive laws. As they are scalable and shiftable, hence to simulate degradation mainly these two properties are used. In case of concrete, compression envelope curve is assumed to be stationary, but at the same time the returning point is assumed to be shifted to simulate the degradation. It means that the point of return on an envelope curve is different to the point where the last reversal occurred from.

b) *Connecting Curves*:

To connect one envelope curve to the other these curves are used. As these curves can also characterize pinching (crack closure), and other softening or hardening phenomena within the material or structural element, so they cannot be represented by single equation. In general more than one equation has to be used to represent this type of curve.

c) *Transition Curves:*

These types of curves are characterized by the connection between two connecting curve. Transition curve is not taken directly to the envelope curve, which can make the model

unstable presenting unwanted shifting under local looping (common on most applications).

1.1.2) Mathematical representation of Transition Curve:

Various types of equations are possible to join two points with a smooth transition curve, but the equation which is most suitable to predict the behavior is derived briefly below. The equation considers six known parameters to find the equation, three for each corresponding to initial and final (target) point. The parameters required are coordinate of intial point (x_o, y_o) with corresponding slope E_o and analogous parameters ((x_f, y_f) and E_f) for final point.

$$y = y_o + E_o(x - x_o) + A(x - x_o)^B \qquad (1)$$

By taking derivative,

$$y' = E_o + AB(x - x_o)^{B-1} \qquad (2)$$

B is assumed to have a value greater than 1, otherwise at $x = x_o$ the first derivative would be indeterminate. Thus,

$$y'(x_o) = E_o \qquad (3)$$

The derivative at the final point should be E_f, then:

$$y'(x_f) = E_f = E_o + AB(x_f - x_o)^{B-1} \qquad (4)$$

and,

$$AB(x_f - x_o)^{B-1} = E_f - E_o \qquad (5)$$

By evaluating the equation (1) at the final point,

3

$$y_f = y_o + E_o(x_f - x_o) + A(x_f - x_o)^B \qquad (6)$$

Or,

$$A(x_f - x_o)^{B-1} = \frac{y_f - y_o}{x_f - x_o} - E_o = E_{sec} - E_o \qquad (7)$$

Using equation (7) and (5),

$$B = \frac{E_f - E_o}{E_{sec} - E_o} \qquad (8)$$

Finally,

$$A = \frac{E_{sec} - E_o}{(x_f - x_o)^{B-1}} \qquad (9)$$

Where,

$$E_{sec} = \frac{y_f - y_o}{x_f - x_f} \qquad (10)$$

The final equation can be written as

$$y = y_o + (x - x_o)\left[E_o + A|x - x_o|^R \right] \qquad (11)$$

Where,

$$R = \frac{E_f - E_{sec}}{E_{sec} - E_o} \qquad (12)$$

$$A = \frac{E_{sec} - E_o}{|x_f - x_o|^R} \qquad (13)$$

and E_{sec} is given by equation (10).

1.1.3) Cyclic Properties of Confined and Unconfined Concrete:

Chang and Mander (1994) developed a cyclic model for confined and unconfined concrete, using the constitutive model of Tsai (1988) as its envelope curve for monotonic loading; which is similar to model proposed by Mander et al(1988a). The model proposed by Mander et al. (1988a) used experimental data of Sinha, Gerstle, and Tulin (1964); and Karsan and Jirsa (1969) to verify the unconfined concrete in cyclic compression. While for confined concrete Mander et al. (1988b) also performed tests to validate the proposed model.

1.1.3.1) Compression Envelope Curve (Rules 1 and 5):

The compression envelope curve can be represented in non-dimensional form by equation described below as shown in Fig. 1. The compression envelope curve is guided by initial Young modulus (E_c), the peak coordinate $(\varepsilon'_{cc}, f'_{cc})$, Tsai's equation factor(r) and non-dimensional critical strain ($x_{cr}^- > 1$). If the stress and tangent Young modulus is written as a function of non-dimensional strain as:

$$f_c = f_c^- \left(x^- \right)^*$$ (14)

$$E_t = E_t^- \left(x^- \right)^*$$ (15)

where the Eqn (14) and (15) can be described in detail as:

For $x^- < x_{cr}^-$ (Tsai's equation - Rule 1)

$$f_c^- = f'_{cc} y(x^-)$$ (16)

$$E_t^- = E_c z(x^-)$$ (17)

For $x_{cr}^- \leq x^- \leq x_{sp}^-$ (straight line - Rule 1)

$$f_c^- = f_{cc}'[y(x_{cr}^-) + n^- z(x_{cr}^-)(x^- - x_{cr}^-)] \tag{18}$$

$$E_t^- = E_c z(x_{cr}^-) \tag{19}$$

For $x_{sp}^- < x^-$ (spalled - Rule 5)

$$f_c^- = E_t^- = 0 \tag{20}$$

where,

$$y(x) = \frac{nx}{D(x)} \quad \text{and} \quad z(x) = \frac{(1 - x^r)}{[D(x)]^2} \tag{21}$$

$$D(x) = 1 + \left(n - \frac{r}{r-1}\right)x + \frac{x^r}{r-1} \quad \text{for } r \neq 1$$

$$= 1 + (n - 1 + \ln x)x \quad \text{for } r = 1 \tag{22}$$

x^- and n^- are defined as: $x^- = \left|\dfrac{\varepsilon_c}{\varepsilon_{cc}'}\right|$ and $n^- = \left|\dfrac{E_c \varepsilon_{cc}'}{f_{cc}'}\right|$ (23)

The spalling non-dimensional strain (x_{sp}) can be calculated as :

$$x_{sp} = x_{cr}^- - \frac{y(x_{cr}^-)}{n^- z(x_{cr}^-)} \tag{24}$$

where,

* - the negative sign (-) refers to parameters related to compression envelope.

E_c = concrete initial Young modulus

E_t = tangent modulus

ε_c = concrete strain

ε_{cc} = concrete strain at peak confined stress

f_c = stress in concrete

f_c^- = concrete stress on the compression envelope

f_{cc} = confined concrete strength

n^- = n value for the compression curve, assumed to be same as that of unconfined concrete.

x^- = non-dimensional strain on the compression envelope

x_{cr}^- = non-dimensional critical strain on the compression envelope curve. This strain is used to define the tangent line up to the spalling strain.

x_{sp} = non-dimensional spalling strain

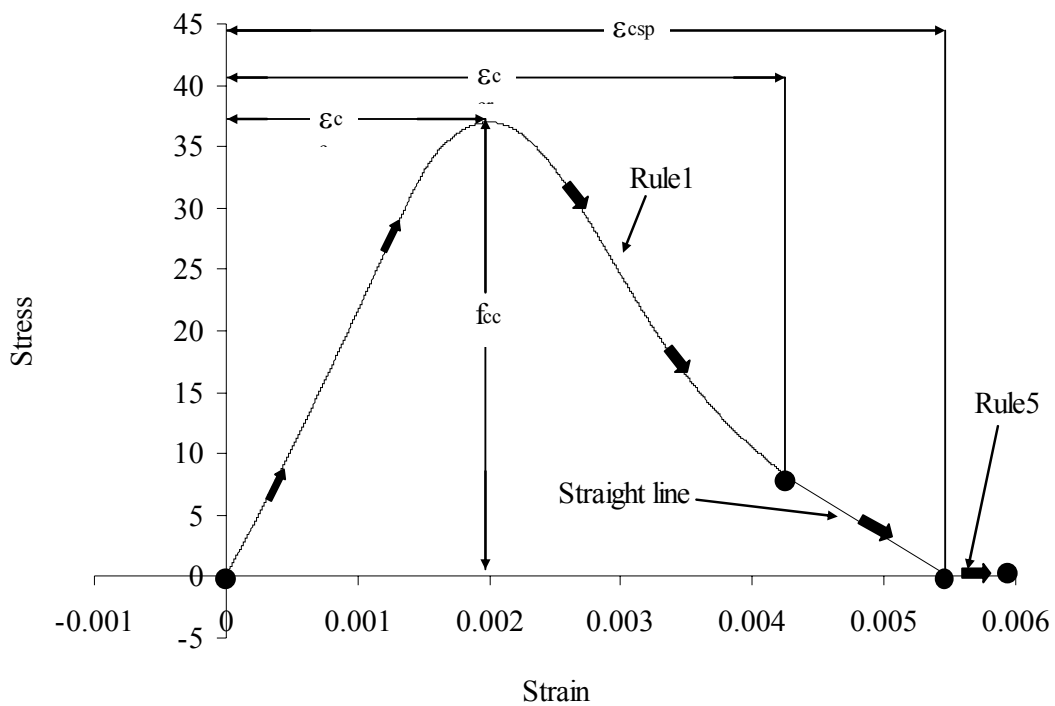$y(x)$ = non-dimensional tangent modulus function

Fig. 1 Representation of rule 1 and rule 5 vital parameters for concrete model.

1.1.3.2) Tension Envelope Curve (Rules 2 and 6):

The shape of tension envelope curve is same as that of the compression envelope curve (Chang and Mander (1994)), hence similar equations can be used to define the rule 2 (Eqn (27-32)) and rule 5 (Eqn (33)) of tension envelope curve. The positive sign (+) refers to the parameters related to the tension side.

To model the degradation on tension side, the curve is shifted to a new origin ε_o (explained in later sections). The non-dimensional parameters n^+, x^+ and x_{crk} (cracking strain) are given by:

$$x^+ = \left| \frac{\varepsilon_c - \varepsilon_o}{\varepsilon_t} \right| \quad \text{and} \quad n^+ = \frac{E_c f_t}{\varepsilon_t} \tag{25}$$

$$x_{crk} = x_{cr}^+ - \frac{y(x_{cr}^+)}{n^+ z(x_{cr}^+)} \tag{26}$$

The stress and tangent modulus for any given strain on the tension envelope curve are similarly defined as:

$$f_c = f_c^+ \left(x^+ \right) \tag{27}$$

$$E_t^+ = E_c z \left(x^+ \right) \tag{28}$$

where $f_c^+ \left(x^+ \right)$ and $E_t^+ \left(x^+ \right)$ can be expressed as:

For $x^+ < x_{cr}^+$ (Rule 2)

$$f_c^+ = f_t y(x^+) \tag{29}$$

$$E_t^+ = E_c z(x^+) \tag{30}$$

8

For $x_{cr}^+ \le x^+ \le x_{crk}^+$ (Rule 2)

$$f_c^+ = f_t[y(x_{cr}^+) + n^+ z(x_{cr}^+)(x^+ - x_{cr}^+)] \tag{31}$$

$$E_t^+ = E_c z(x_{cr}^+) \tag{32}$$

For $x_{crk}^+ < x^+$ (Rule 6)

$$f_c^+ = E_t^+ = 0 \tag{33}$$

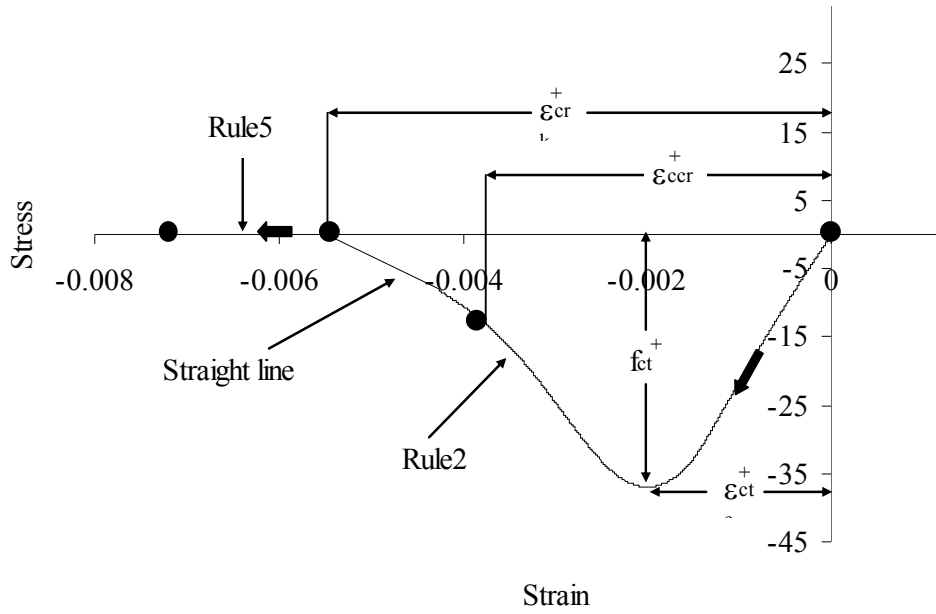
Fig. 2 Representation of rule 2 and rule 6 (not to scale , hypothetical data for

reprsentation).

ε_t = strain at peak tension stress

f_t = concrete tension strength

x^+ = non-dimensional strain in the tension envelope curve

9

$n^+ = n$ value for the tension envelope curve

$x_{cr}^+ =$ critical strain on the tension envelope curve. This factor is used to define the cracking strain.

Where functions y and z are defined by Eqn (21). When the concrete has cracked it is assumed that it will be having no tension resistance capacity, as a result of crack opening; but on the other hand a gradual crack closure can lead to compressive stress.

1.1.3.3) Intermediate Parameters:

The current section deals with the intermediate parameters required for the hysteretic laws. The Eqn 11 is used for the transition curve described in the coming sections in the form represented as:

$$f_c = f_i + (\varepsilon_c - \varepsilon_i)[E_i + A|\varepsilon_c - \varepsilon_i|^R] \tag{34}$$

where

$$E_{sec} = \frac{y_f - y_i}{x_f - x_i}, \quad R = \frac{E_f - E_{sec}}{E_{sec} - E_i} \quad \text{and} \quad A = \frac{E_{sec} - E_i}{|x_f - x_i|^R}$$

subscripts i, f and sec indicate initial, final and secant respectively.

The hysteretic parameters required for cyclic compression are described by:

$$E_{sec}^- = E_c \left(\frac{\left|\frac{f_{un}^-}{E_c \varepsilon_{cc}'}\right| + 0.57}{\left|\frac{\varepsilon_{un}^-}{\varepsilon_{cc}'}\right| + 0.57} \right) \tag{35}$$

$$E_{pl}^- = 0.1 E_c \exp\left(-2\left|\frac{\varepsilon_{un}^-}{\varepsilon_{cc}'}\right|\right) \tag{36}$$

$$\Box\varepsilon^- = \frac{\varepsilon_{un}^-}{1.15 + 2.75\left|\frac{\varepsilon_{un}^-}{\varepsilon_{cc}'}\right|} \tag{37}$$

$$\Delta f^- = 0.09 f_{un}^- \sqrt{\left|\frac{\varepsilon_{un}^-}{\varepsilon_{cc}'}\right|} \tag{38}$$

$$\varepsilon_{pl}^- = \varepsilon_{un}^- - \frac{f_{un}^-}{E_{sec}^-} \tag{39}$$

$$f_{new}^- = f_{un}^- - \Delta f^- \tag{40}$$

$$E_{new}^- = \frac{f_{new}^-}{\varepsilon_{un}^- - \varepsilon_{pl}^-} \tag{41}$$

$$\varepsilon_{re}^- = \varepsilon_{un}^- + \Delta\varepsilon^- \tag{42}$$

$$f_{re}^- = f^-\left(\left|\frac{\varepsilon_{re}^-}{\varepsilon_{cc}'}\right|\right) \tag{43}$$

$$E_{re}^- = E^-\left(\left|\frac{\varepsilon_{re}^-}{\varepsilon_{cc}'}\right|\right) \tag{44}$$

Similarly the parameters required for cyclic tension are given by:

$$E_{sec}^+ = E_c\left(\frac{\left|\frac{f_{un}^+}{E_c\varepsilon_t}\right| + 0.67}{\left|\frac{\varepsilon_{un}^+ - \varepsilon_o}{\varepsilon_t}\right| + 0.67}\right) \tag{45}$$

$$E_{pl}^+ = \frac{E_c}{\left|\frac{\varepsilon_{un}^+ - \varepsilon_o}{\varepsilon_t}\right|^{1.1} + 1} \tag{46}$$

$$\Box\varepsilon^+ = 0.22\varepsilon_{un}^+ \tag{47}$$

11

$$\Delta f^+ = 0.15 f_{un}^+ \tag{48}$$

$$\varepsilon_{pl}^+ = \varepsilon_{un}^+ - \frac{f_{un}^+}{E_{sec}^+} \tag{49}$$

$$f_{new}^+ = f_{un}^+ - \Delta f^+ \tag{50}$$

$$E_{new}^+ = \frac{f_{new}^+}{\varepsilon_{un}^+ - \varepsilon_{pl}^+} \tag{51}$$

$$\varepsilon_{re}^+ = \varepsilon_{un}^+ + \Delta\varepsilon^+ \tag{52}$$

$$f_{re}^+ = f^+ \left(\left| \frac{\varepsilon_{re}^+ - \varepsilon_o}{\varepsilon_t} \right| \right) \tag{53}$$

$$E_{re}^+ = E^+ \left(\left| \frac{\varepsilon_{re}^+ - \varepsilon_o}{\varepsilon_t} \right| \right) \tag{54}$$

where,

ε_{un} = unloading strain from an envelope curve

f_{un} = unloading stress

ε_{pl} = plastic strain

E_{pl} = tangent modulus when the stress is released

f_{new} = new stress at the unloading strain

E_{new} = tangent modulus at the new stress point

ε_{re} = strain at the returning point to the envelope curve

f_{re} = stress at the returning point

E_{re} = tangent modulus at the returning point

1.1.3.4) Calculation of shift for Tension envelope curve:

The shift in tension envelope curve is calculated as described in following steps:

(a) Calculate compression and tension strain ductility as:

$$x_u^- = \left| \frac{\varepsilon_{un}^-}{\varepsilon_{cc}'} \right| \quad \text{and} \quad x_u^+ = \left| \frac{\varepsilon_{un}^+ - \varepsilon_o}{\varepsilon_t} \right|$$

(b) If $x_u^+ < x_u^-$ then:

$$x_u^+ = x_u^-,$$

$$\varepsilon_o = 0,$$

$$\varepsilon_{un}^+ = x_u^+ \varepsilon_t \text{ and}$$

find corresponding stress f_{un}^+ from tensile envelope curve for the strain (ε_{un}^+) from

Eqn.(27) and calculate $\Delta\varepsilon_o = \dfrac{2f_{un}^+}{E_{sec}^+ + E_{pl}^-}$.

(c)The shift is calculated by

$$\varepsilon_o = \varepsilon_{pl}^- + \Delta\varepsilon_o - x_u^+ \varepsilon_t \tag{55}$$

3.4) Reversal from Compression envelope curve:

A reversal from compression envelope curve begins with rule 3, which subsequently make over to rule 8 through rule 9 as intermediate rule, to finally end on tension envelope curve. All the rules use the Eq (34) to connect smoothly the initial and final point. The rules are described in Fig (3), with the parameters required for Eq. (34) described below in tabular form.

Parameters	Rule 3	Rule 9	Rule 8
ε_i	ε_{un}^-	ε_{pl}^-	ε_{un}^+
f_i	f_{un}^-	0	f_{new}^+

E_i	E_c	E_{pl}^-	E_{new}^+
ε_f	ε_{pl}^-	ε_{un}^+	ε_{re}^+
f_f	0	f_{new}^+	f_{re}^+
E_f	E_{pl}^-	E_{new}^+	E_{re}^+

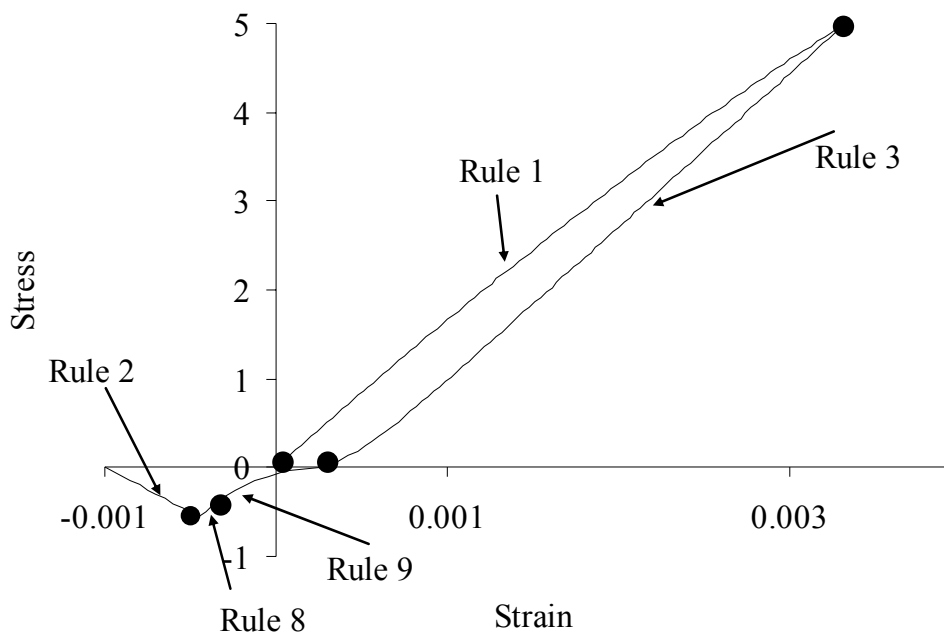Fig. 3 Reversal from compression envelope curve (hypothetical data used fro

representation).

1.1.3.4) Reversal from Tension envelope curve:

The reversal from tension envelope curve is similar to the reversal from compression, while the rule 4, rule 10 and rule 7 are used, which are also described in Fig(4). The rules are summarized in tabular form:

Parameters	Rule 4	Rule 10	Rule 7

ε_i	ε_{un}^+	ε_{pl}^+	ε_{un}^-
f_i	f_{un}^+	0	f_{new}^-
E_i	E_c	E_{pl}^+	E_{new}^-
ε_f	ε_{pl}^+	ε_{un}^-	ε_{re}^-
f_f	0	f_{new}^-	f_{re}^-
E_f	E_{pl}^+	E_{new}^-	E_{re}^-

Fig. 4.1 Reversal from Tension envelope curve.
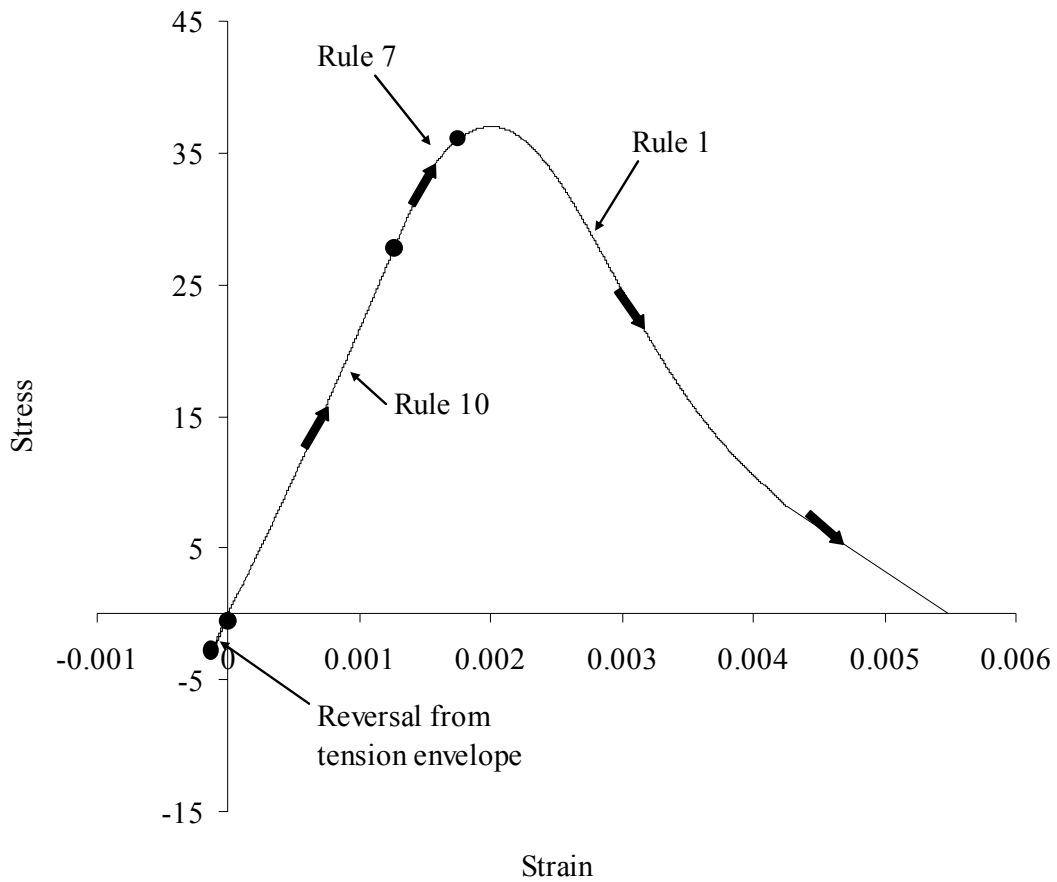
Fig. 4.2 Reversal from Tension envelope curve.

1.1.3.5)Post cracking unloading and reloading curves:

When complete cracking occurs, then it is understood that there will be no tensile resistance capacity, so the region corresponding to tension will also not exist. When reversal from compression envelope curve will occur, rule 6 will follow rule 3 instead of rule 9 and rule 8. Reversal from rule 6 in this case will be followed by rule 13 (Fig 5). The parameter describing rule 13 are described in tabular form:

Parameters	Rule 13

ε_i	ε_r
f_i	0
E_i	0
ε_f	ε_{un}^-
f_f	$\tilde{f}_{new}$
E_f	E_{new}^-

where ε_r corresponds to reversal strain from rule 6.

1.1.3.6) Pre- cracking transition curves:

Rules 3, 4, 9 and 10 are considered as connecting curves, whenever reversal occurs from these rules, a transition curve is used to connect to envelope curves or connecting curves. Each rule is dealt separately below and compared with its counterpart.

When reversal from rule 3 occurs, modified rule 7 is used. In this case $\tilde{f}_{new}$ is modified to f_{new}^-*; and the returning point coordinate $(\varepsilon_{re}^-, f_{re}^-)$ are also changed to $(\varepsilon_{re}^-*, f_{re}^-*)$. The modified expressions are:

$$f_{new*}^- = f_{un}^- - \Delta f^- \frac{\varepsilon_{un}^- - \varepsilon_{ro}^-}{\varepsilon_{un}^- - \varepsilon_{pl}^-} \tag{56}$$

$$E_{new*}^- = \frac{f_{new*}^- - f_{ro}^-}{\varepsilon_{un}^- - \varepsilon_{ro}^-} \tag{57}$$

$$\varepsilon_{re*}^- = \varepsilon_{un}^- + \Delta\varepsilon^- \frac{\varepsilon_{un}^- - \varepsilon_{ro}^-}{\varepsilon_{un}^- - \varepsilon_{pl}^-} \tag{58}$$

$$f_{re*}^- = f^- \left(\left| \frac{\varepsilon_{re*}^-}{\varepsilon_{cc}} \right| \right) \tag{59}$$

$$E_{re*}^- = E^- \left(\left| \frac{\varepsilon_{re*}^-}{\varepsilon_{cc}} \right| \right) \tag{60}$$

The modified rule 7 (rule 7*) is described in tabular form for the possible strains as:

Parameters	$\left|\varepsilon_{ro}^-\right| \leq \left|\varepsilon_c^-\right| \leq \left|\varepsilon_{un}^-\right|$	$\left|\varepsilon_{un}^-\right| < \left|\varepsilon_c^-\right| < \left|\varepsilon_{re*}^-\right|$
ε_i	ε_{ro}^-	ε_{un}^-
f_i	f_{ro}^-	f_{new}^- *
E_i	E_c	E_{new*}^-
ε_f	ε_{un}^-	ε_{re}^- *
f_f	f_{new}^- *	f_{re}^- *
E_f	E_{new*}^-	E_{re}^- *

Similarly rule 8 is modified to rule 8*, when reversal from rule 4 occurs. The parameters

required for rule 8* is described in tabular from as:

$$f_{new*}^+ = f_{un}^+ - \Delta f^+ \frac{\varepsilon_{un}^+ - \varepsilon_{ro}^+}{\varepsilon_{un}^+ - \varepsilon_{pl}^+} \tag{61}$$

$$E_{new*}^+ = \frac{f_{new}^+ - f_{ro}^+}{\varepsilon_{un}^+ - \varepsilon_{ro}^+} \tag{62}$$

$$\varepsilon_{re*}^+ = \varepsilon_{un}^+ + \Delta \varepsilon^+ \frac{\varepsilon_{un}^+ - \varepsilon_{ro}^+}{\varepsilon_{un}^+ - \varepsilon_{pl}^+} \tag{63}$$

$$f_{re*}^+ = f^+ \left(\left| \frac{\varepsilon_{re*}^+ - \varepsilon_o}{\varepsilon_t} \right| \right) \tag{64}$$

$$E_{re*}^+ = E^+ \left(\left| \frac{\varepsilon_{re*}^+ - \varepsilon_o}{\varepsilon_t} \right| \right) \tag{65}$$

Similar to rule 7* rule 8* can be described as:

Parameters	$\left\|\varepsilon_{ro}^+ - \varepsilon_o\right\| \le \left\|\varepsilon_c - \varepsilon_o\right\| \le \left\|\varepsilon_{un}^+ - \varepsilon_o\right\|$	$\left\|\varepsilon_{un}^+ - \varepsilon_o\right\| < \left\|\varepsilon_c - \varepsilon_o\right\| < \left\|\varepsilon_{re*}^+ - \varepsilon_o\right\|$
ε_i	ε_{ro}^+	ε_{un}^+
f_i	f_{ro}^+	$f_{new}^+ *$
E_i	E_c	E_{new*}^+
ε_f	ε_{un}^+	$\varepsilon_{re}^+ *$
f_f	$f_{new}^+ *$	$f_{re}^+ *$
E_f	E_{new*}^+	$E_{re}^+ *$

When reversal from rule 9 occurs from point **a** (ε_a, f_a), it is considered that it will target rule 10 at point **b** (ε_b, f_b), via rule 11 and analogous case will exist for rule 10; except rule 9 will be targeted at point **a** (ε_a, f_a), via rule 12. The relation between **a** (ε_a, f_a), and **b** (ε_b, f_b) is given by

$$\frac{\varepsilon_a - \varepsilon_{pl}^-}{\varepsilon_{un}^+ - \varepsilon_{pl}^-} = \frac{\varepsilon_{un}^- - \varepsilon_b}{\varepsilon_{un}^- - \varepsilon_{pl}^+} \tag{66}$$

Rule 11 and 12 are expressed in tabular form as:

Parameters	Rule 11	Rule 12
ε_i	ε_r	ε_r
f_i	f_r	f_r
E_i	E_c	E_c
ε_f	ε_b	ε_a

$\boldsymbol{f}_f$	f_b	f_a
$\boldsymbol{E}_f$	$E_t(\varepsilon_b)$	$E_t(\varepsilon_a)$

where, (ε_r, f_r) represents most recent reversal coordinate.

1.1.3.7) Post- cracking transition curves:

When cracking is considered, the existence of tension envelope curve diminishes; hence any reversal from rule 13 can target only the strain axis. If a reversal occur from rule 13 from **a** (ε_a, f_a), it will target **b** $(\varepsilon_b, 0)$ through rule 14. A reversal from rule 14 will target rule 13 at point **a** (ε_a, f_a) through rule 15. The relation among **a** (ε_a, f_a) and **b** (ε_b, f_b) is given by:

$$\varepsilon_b = \varepsilon_a - \frac{f_a}{E_{sec}^-} \tag{67}$$

The rule 14 and 15 are described in tabular form as:

Parameters	Rule 11	Rule 12
ε_i	ε_r	ε_r
$\boldsymbol{f}_i$	f_r	f_r
$\boldsymbol{E}_i$	E_c	E_c
ε_f	ε_b	ε_a
$\boldsymbol{f}_f$	0	f_a
$\boldsymbol{E}_f$	0	$E_t(\varepsilon_a)$

where, (ε_r, f_r) represents most recent reversal coordinate.

1.2 STEEL CONSTITUTIVE CYCLIC LAWS

The constitutive laws described in this section are taken from Chang and Mander (1994)

Chang and Mander(1994) calibrated the proposed laws from the experimental results obtained from Kent and Park (1973), Ma et al. (1976), and Panthaki (1991). The loading and unloading stress-strain curves are being characterized by the Menegotto-Pinto equation (1973).

1.2.1)The Menegotto-Pinto Equation:

The Menegotto-Pinto equation (M-P hereafter) describes a curve connecting two tangents with a variable radius of curvature at the intersection point of these tangents. The M-P equation describing a curve (Fig. 8) joining the initial point (ε_o, f_o) and final point (ε_f, f_f) can be represented as follows:

$$f_s = f_o + E_o(\varepsilon_s - \varepsilon_o) \left\{ Q + \frac{1-Q}{\left[1 + \left| E_o \frac{\varepsilon_s - \varepsilon_o}{f_{ch} - f_o} \right|^R \right]^{\frac{1}{R}}} \right\} \tag{68}$$

The tangent modulus at any point is given by:

$$E_t = \frac{\partial f_s}{\partial \varepsilon_s} = E_{sec} - \frac{E_{sec} - QE_o}{1 + \left| E_o \frac{\varepsilon_s - \varepsilon_o}{f_{ch} - f_o} \right|^{-R}} \tag{69}$$

where:

f_s = stress in steel

f_o = stress in steel at initial point of the curve

E_o = tangent modulus at initial point of the curve

21

ε_s = strain in steel

ε_o = strain in steel at initial point of the curve

Q = an equation parameter to control the shape of the curve

f_{ch} = an equation parameter to control the shape of the curve

R = an equation parameter to control the shape of the curve

E_t = tangent modulus of steel

E_{sec} = secant modulus or the slope of the line connecting the initial point (ε_o, f_o) and the

final point (ε_f, f_f)

1.2.2)Algorithm of M-P Equation:

The following steps are involved in determining the unknown parameters of M-P

equation.

1) Calculate E_{sec} as:

$$E_{sec} = \frac{f_f - f_o}{\varepsilon_f - \varepsilon_o} \tag{70}$$

2) Calculate R_{min} as:

$$R_{min} = \frac{E_f - E_{sec}}{E_{sec} - E_o} \tag{71}$$

3) If $R_{min} = 0$, the value of Q is taken as 1. In this case $f_{ch} = f_f$

4) If $R \le R_{min}$ then take $R = R_{min} + 0.01$

5) Define a function of variable a :

$$f(a) = E_f - E_{sec} \frac{1 - a^{R+1}}{1 - a} + E_o \frac{a(1 - a^R)}{1 - a} \tag{72}$$

6) Take $z = 0.01$. Calculate $f(1 - z) \times f(z)$

7) Decrease the value of z until $f(1-z) \times f(z)$ becomes ≤ 0. Once this condition is reached, the value of a satisfying the following equation can be found in the interval $(0, z)$. The equation to be satisfied is:

$$E_f - E_{\text{sec}} \frac{1-a^{R+1}}{1-a} + E_o \frac{a(1-a^R)}{1-a} = 0 \qquad (73)$$

8) Consider an initial estimate:

$$a_o = \frac{R_{\min}}{R} \qquad (74)$$

9) Calculate $f(a_o) \times f(1-\varepsilon)$ and if this is < 0 then decrease the value of a_o using the following recursive function:

$$a_{i+1} = a_i - \frac{2f(a_i)\Delta a}{f(a_i + \Delta a) - f(a_i - \Delta a)} \qquad (75)$$

This recursion should be applied on a until the value of $f(a_o) \times f(1-\varepsilon) \geq 0$

The value of Δa should be taken as:

$$\Delta a = \min \left\{ \begin{matrix} 0.5(1-a_o) \\ 0.001 \end{matrix} \right\} \qquad (76)$$

10) Once the desired value of a is obtained, the value of unknown parameter b can be calculated as:

$$b = \frac{(1-a^R)^{\frac{1}{R}}}{a} \qquad (77)$$

The parameters a and b are used in calculating the values of the unknown M-P parameters f_{ch} and Q.

11) Using the known values of a and b the value of f_{ch} and Q can be calculated as:

$$f_{ch} = f_o + \frac{E_o}{b}(\varepsilon_f - \varepsilon_o) \qquad (78)$$

$$Q = \frac{\dfrac{E_{\text{sec}}}{E_o} - a}{1 - a}$$

(79)

12) Using these obtained values of initially unknown parameters b, f_{ch}, Q the value of f_s corresponding to the value of ε_s can be calculated from Eqn (68) and the value of tangent modulus E_t can be obtained from Eqn (69).

1.2.3.1) Cyclic properties of Reinforcing Steel:

This section deals with the stress-strain model for ordinary reinforcing and high strength prestressing bars. It is described by ten rules, five corresponding to tension and other five for the compression

1.2.3.2) Envelope Branches (Rule 1 and Rule 2):

The envelope branches are composed of monotonic stress-strain relation along both the tension and the compression side, known as a) Tension Envelope Branch and b) Compression Envelope Branch.

Rule 1 (Tension Envelope Branch): Chang and Mander(1994) assumed that the form of the envelope branches should be kept intact, but when reversal would occur from them, a scale factor would be considered. The model proposed the degradation of steel under the action of local cyclic loading, which has not been proposed before. Chang and Mander (1994) validated their model by means of experimental results obtained by Panthaki (1991). The stress-strain relationship for the tension envelope curve is represented in (Fig. 8) and expressed by:

24

$$f_s = \frac{E_s \varepsilon_{ss}}{\left[1 + \left(\dfrac{E_s \varepsilon_{ss}}{f_y^+} \right)^{10} \right]^{0.1}} + \frac{sign(\varepsilon_{ss} - \varepsilon_{sh}^+) + 1}{2} (f_{su}^+ - f_y^+) \left[1 - \left| \frac{\varepsilon_{su}^+ - \varepsilon_{ss}}{\varepsilon_{su}^+ - \varepsilon_{sh}^+} \right|^{p+} \right] \tag{80}$$

$$E_t = \frac{E_s}{\left[1 + \left(\dfrac{E_s \varepsilon_{ss}}{f_y^+} \right)^{10} \right]^{1.1}} + \frac{sign(\varepsilon_{ss} - \varepsilon_{sh}^+) + 1}{2} sign(\varepsilon_{su}^+ - \varepsilon_{ss}) E_{sh}^+ \left| \frac{f_{su}^+ - f_s}{f_{su}^+ - f_y^+} \right|^{\frac{p^+ - 1}{p^+}} \tag{81}$$

where:

$$\varepsilon_{ss} = \varepsilon_s - \varepsilon_{om}^+ \tag{82}$$

$$p^+ = E_{sh}^+ \frac{\varepsilon_{su}^+ - \varepsilon_{sh}^+}{f_{su}^+ - f_y^+} \tag{83}$$

and

ε_{om}^+ = point of origin of the tension envelope branch

E_s = Elastic modulus of Elasticity

f_y^+ = yield stress during tension in steel

ε_{sh}^+ = strain hardening strain during tension in steel

f_{su}^+ = ultimate (maximum) stress during tension in steel

ε_{su}^+ = strain at ultimate stress in steel during tension in steel

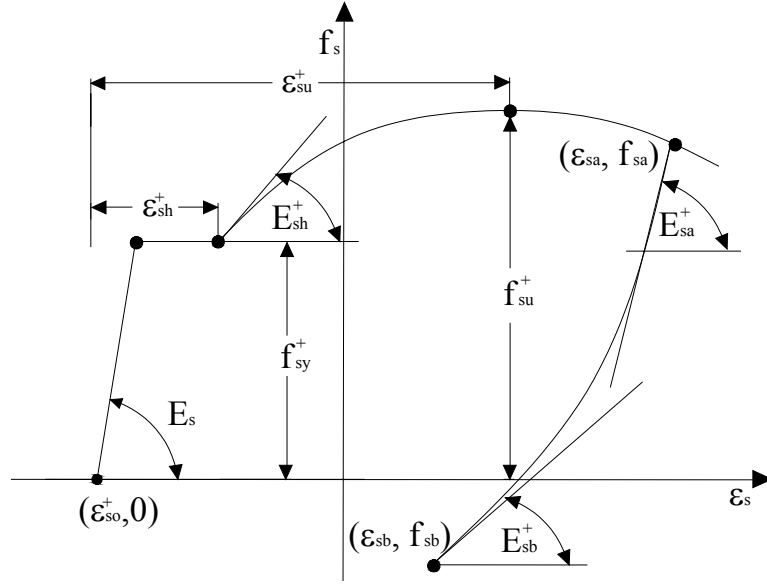E_{sh}^+ = tangent modulus at strain hardening

Fig. 8 Representation of vital parameters for steel model.

Rule 2 (Compression Envelope Branch): The governing equations for the compression envelope curve are described as:

$$f_s = \frac{E_s \varepsilon_{ss}}{\left[1+\left(\dfrac{E_s \varepsilon_{ss}}{f_y^-}\right)^{10}\right]^{0.1}} + \frac{sign(\varepsilon_{sh}^- - \varepsilon_{ss})+1}{2}(f_{su}^- - f_y^-)\left[1-\left|\frac{\varepsilon_{su}^- - \varepsilon_{ss}}{\varepsilon_{su}^- - \varepsilon_{sh}^-}\right|^{p^-}\right] \tag{84}$$

$$E_t = \frac{E_s}{\left[1+\left(\dfrac{E_s \varepsilon_{ss}}{f_y^-}\right)^{10}\right]^{1.1}} + \frac{sign(\varepsilon_{sh}^- - \varepsilon_{ss})+1}{2} sign(\varepsilon_{ss} - \varepsilon_{su}^-)E_{sh}^- \left|\frac{f_{su}^- - f_s}{f_{su}^- - f_y^-}\right|^{\frac{p^- -1}{p^-}} \tag{85}$$

where:

$$\varepsilon_{ss} = \varepsilon_s - \varepsilon_{om}^- \tag{86}$$

$$p^- = E_{sh}^- \frac{\varepsilon_{su}^- - \varepsilon_{sh}^-}{f_{su}^- - f_y^-} \tag{87}$$

26

and,

ε_{om}^- = point of origin of the compression envelope branch

f_y^- = yield stress during compression in steel

ε_{sh}^- = strain hardening strain during compression in steel

f_{su}^- = ultimate (maximum) stress during compression in steel

ε_{su}^- = strain at ultimate stress in steel during compression in steel

E_{sh}^- = tangent modulus at strain hardening

1.2.3.3) Reversal Branches (Rule 3 and Rule 4): The curve which connects a reversal point on an envelope branch with a target point on the opposite envelope branch is known as a reversal branch. It is considered that a reversal branch can be exclusively described by the two extreme points:

a) Maximum excursion into the tension envelope branch (ε_{max})

b) Maximum excursion into the compression envelope branch (ε_{min})

The type of reversal can be categorized in two cases depending on the position of reversal point:

      a) Reversal from a point within the yield plateau

      b) Reversal from a point on the strain hardened curve.

These two cases are considered separately as they are governed by different set of equations.

The reversal branches can also be divided into two types:

      a) Unloading Reversal Branch (Rule 3)

      b) Loading Reversal Branch (Rule 4)

Rule 3 (Unloading Reversal Branch):

<u>Case1</u>**:** If the unloading starts at a point (ε_o^-, f_o^-) on the tension envelope curve within the yield plateau (Fig.9) then following equations are used to calculate intermediate parameters for unloading. The target strain (ε_{ta}^-) on the compressive envelope branch is calculated as:

$$\varepsilon_{max} = \varepsilon_o^- - \varepsilon_{om}^+ \tag{88}$$

$$\varepsilon_{ta}^- = \varepsilon_{om}^- + \varepsilon_{min} \tag{89}$$

where,

$$\tag{90}$$

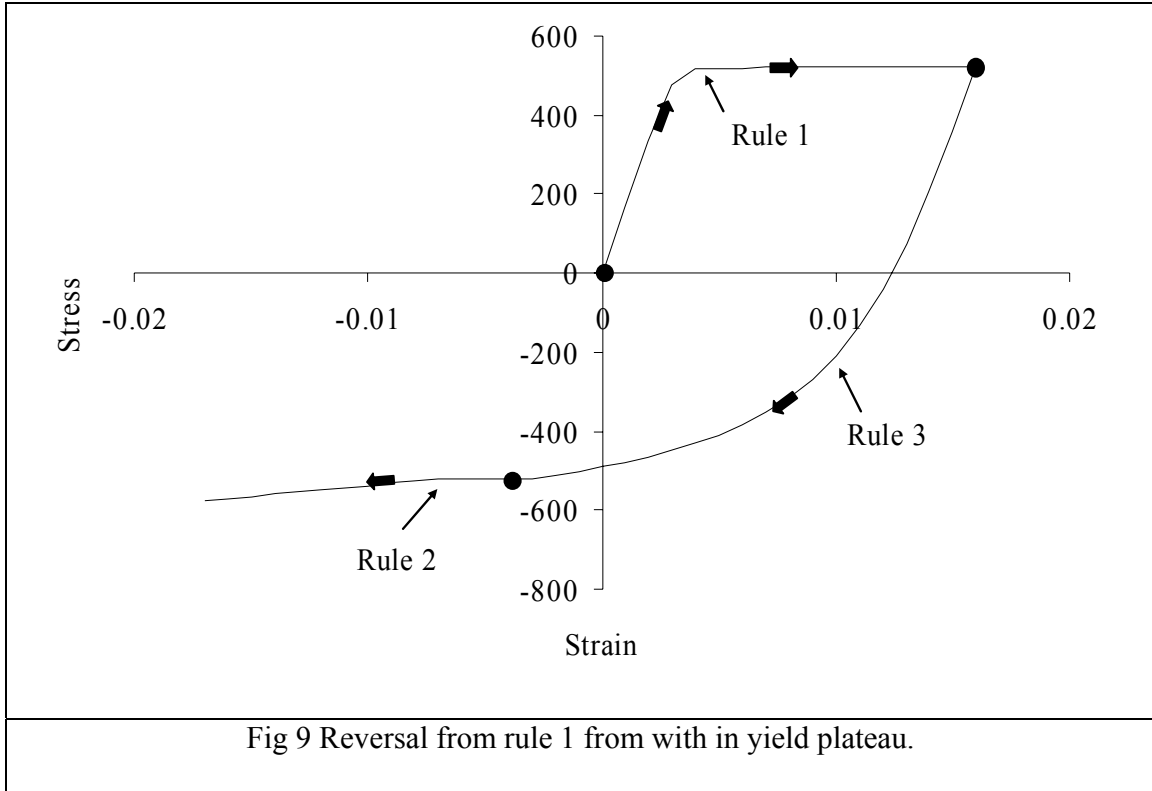$$\varepsilon_{min} = \varepsilon_y^- + p_r\left(\varepsilon_{sh}^- - \varepsilon_y^-\right)$$

$$\varepsilon_{om}^- = \varepsilon_o^- - \frac{f_o^-}{E_s} \tag{91}$$

$$p_r = \frac{\varepsilon_{max} - \varepsilon_y^+}{\varepsilon_{sh}^+ - \varepsilon_y^+} \tag{92}$$

The target slope is calculated by:

$$E_{ta}^- = \frac{1}{\dfrac{1}{E_s} + p_r\left(\dfrac{1}{E_{sh}^-} - \dfrac{1}{E_s}\right)} \tag{93}$$

The target stress f_{ta}^- is the yield stress (f_y^-) on the compression envelope branch.

Fig 9 Reversal from rule 1 from with in yield plateau.

Case 2: If the unloading starts at a point (ε_o^-, f_o^-) on the strain hardening curve (Fig.10) then following equations are used to calculate intermediate parameters for unloading. The ε_{min} is calculated in same manner as in equation (90), but it should satisfy the following condition:

$$|\varepsilon_{min}| > |\varepsilon_{sh}^-| \tag{94}$$

The shifted origin for the compression envelope branch on strain axis is calculated as:

$$\varepsilon_{om}^- = \varepsilon_a^+ k_{rev}^- + \varepsilon_b^+(1 - k_{rev}^-) \tag{95}$$

where:

$$\varepsilon_a^+ = \varepsilon_{om}^+ + \varepsilon_{sh}^+ - \frac{f_y^+}{E_s} \tag{96}$$

$$\varepsilon_b^+ = \varepsilon_{om}^+ + \varepsilon_{max} - \frac{f_{max}}{E_s} \tag{97}$$

$$k_{rev}^- = \exp\left(-\frac{\varepsilon_{max}}{5000(\varepsilon_y^+)^2}\right) \tag{98}$$

with:

k_{rev}^- = A factor used to locate the compression envelope branch between the points ε_a^+

and ε_b^+.

The target strain ε_{ta}^- is calculated using Eqn (89).

In this case the target stress f_{ta}^- and target slope E_{ta}^- are calculated from equations (84) and

(85) respectively. The controlling parameters used in the MP equation are shown in

tabular form below:

Parameters	Rule 3
ε_{a3}	$\varepsilon_{om}^+ + \varepsilon_{max}$
f_{a3}	f_{max}
E_{a3}	E_o^-
ε_{b3}	ε_{ta}^-
f_{b3}	f_{ta}^-
E_{b3}	E_{ta}^-

where:

ε_{a3} = Starting strain of Rule 3

f_{a3} = Starting stress of Rule 3

E_{a3} = Starting slope of Rule 3

ε_{b3} = Target strain of Rule 3

f_{b3} = Target stress of Rule 3
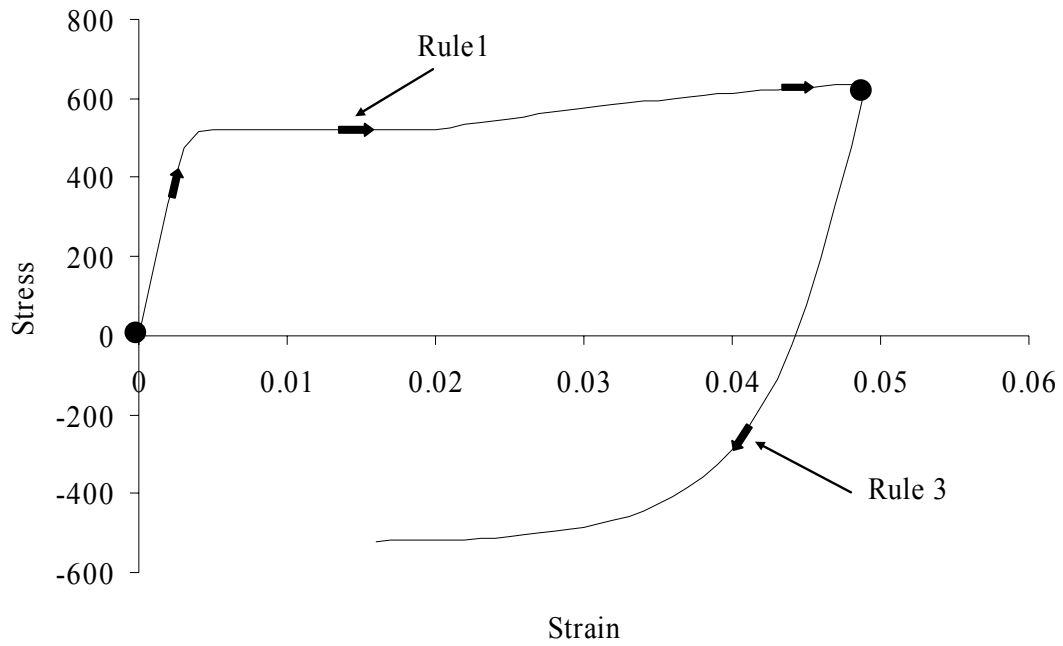
E_{b3} = Target slope of Rule 3

Fig 10 Reversal from rule 1 after strain hardening

The initial slope E_o^- and the Menegotto-Pinto equation parameter R^- are the functions of

the strain amplitude $\Delta\varepsilon_a$ which is given by:

$$\Delta\varepsilon_a = \frac{\varepsilon_{b3} - \varepsilon_{a3}}{2} \qquad (99)$$

Experiments carried out by Panthaki (1991) have shown that the initial Young's modulus

at the unloading point can be expressed as:

$$E_o^- = (1 - 3\Delta\varepsilon_a)E_s \tag{100}$$

The M-P parameter R was also found to be a function of the yield stress, which can be expressed as:

$$R^- = 16\left(\frac{f_y}{E_s}\right)^{\frac{1}{3}}(1 - 10\Delta\varepsilon_a) \tag{101}$$

Using these parameters the M-P equation can be used to derive the unloading reversal curve i.e. the Rule 3. Fig. 10 shows the transition from Rule 1 to Rule 3 obtained from the numerical simulation of the hysteretic model for steel reinforcing bars.

Rule 4 (Loading Reversal Branch):

Case1: If the reversal crops up from a point (ε_o^+, f_o^+) lying within the yield plateau of the compression envelope branch, the following equations govern the loading reversal curve:

$$\varepsilon_{\min} = \varepsilon_o^+ - \varepsilon_{om}^- \tag{102}$$

The target strain on the tension envelope branch is calculated as:

$$\varepsilon_{ta}^+ = \varepsilon_{om}^+ + \varepsilon_{\max} \tag{103}$$

where,
$$\varepsilon_{\max} = \varepsilon_y^+ + p_r(\varepsilon_{sh}^+ - \varepsilon_y^+) \tag{104}$$

$$\varepsilon_{om}^+ = \varepsilon_o^+ - \frac{f_o^+}{E_s} \tag{105}$$

$$p_r = \frac{\varepsilon_{\min} - \varepsilon_y^-}{\varepsilon_{sh}^- - \varepsilon_y^-} \tag{106}$$

The target slope is calculated by:
$$E_{ta}^+ = \frac{1}{\dfrac{1}{E_s} + p_r\left(\dfrac{1}{E_{sh}^+} - \dfrac{1}{E_s}\right)} \tag{107}$$

The target stress f_{ta}^+ is the yield stress f_y^+ on the tension envelope branch.
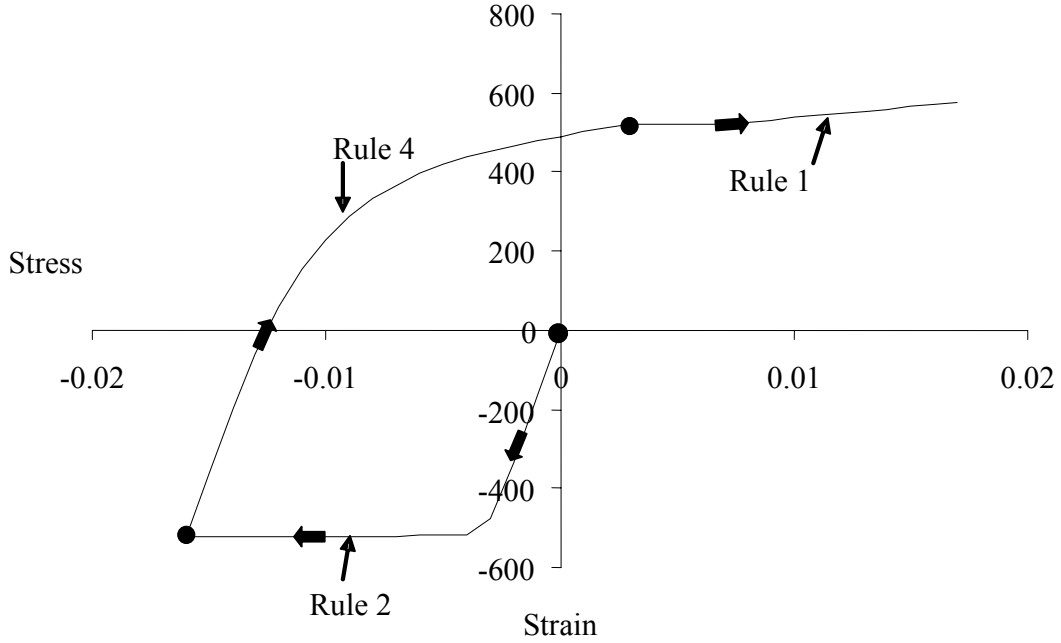

Fig 11 Reversal from rule 2 from with in yield plateau.

Case2: If the reversal takes place from a point on the strain hardening curve (Fig. 12) then the following equations govern the loading reversal curve. The ε_{max} is calculated in same manner as in equation (104)

The shifted origin abscissa for the tension envelope branch is calculated as:

$$\varepsilon_{om}^+ = \varepsilon_a^-(1-k_{rev}^+) + \varepsilon_b^- k_{rev}^+)$$

(108)

where:

$$\varepsilon_a^- = \varepsilon_{om}^- + \varepsilon_{sh}^- - \frac{f_y^-}{E_s}$$

(109)

$$\varepsilon_b^- = \varepsilon_{om}^- + \varepsilon_{min} - \frac{f_{min}}{E_s}$$

(110)

33

$$\begin{array}{|l|r|}
\hline
k_{rev}^+ = \exp\left(-\dfrac{|\varepsilon_{min}|}{5000(\varepsilon_y^-)^2}\right) & (111) \\
\hline
\end{array}$$

With:

k_{rev}^+ = A factor used to locate the tension envelope branch between the points ε_a^- and ε_b^-.

The target strain ε_{ta}^+ is calculated using equation (103).

In this case the target stress f_{ta}^+ and target slope E_{ta}^+ are calculated from equations (113) and (114) respectively.

The starting strain, stress, slope and the target strain, stress, slope for Rule 4 are defined by the following equations:

Parameters	Rule 4
ε_{a4}	$\varepsilon_{om}^- + \varepsilon_{min}$
f_{a4}	f_{min}
E_{a4}	E_o^+
ε_{b4}	ε_{ta}^+
f_{b4}	f_{ta}^+
E_{b4}	E_{ta}^+

where:

The initial slope E_o^+ and the Menegotto-Pinto equation parameter R^+ are the functions of the strain amplitude $\Delta\varepsilon_a$ which is given by:

$$\Delta\varepsilon_a = \left|\frac{\varepsilon_{b4} - \varepsilon_{a4}}{2}\right| \qquad (112)$$

Experiments performed by Panthaki (1991) have shown that the initial Young's modulus at the point of reversal from the compression envelope branch (loading) can be expressed as:

$$E_o^+ = (1 - \Delta\varepsilon_a)E_s \tag{113}$$

The M-P parameter R was also found to be a function of the yield stress, which can be expressed as:

$$R^+ = 20\left(\frac{f_y}{E_s}\right)^{\frac{1}{3}}(1 - 20\Delta\varepsilon_a) \tag{114}$$
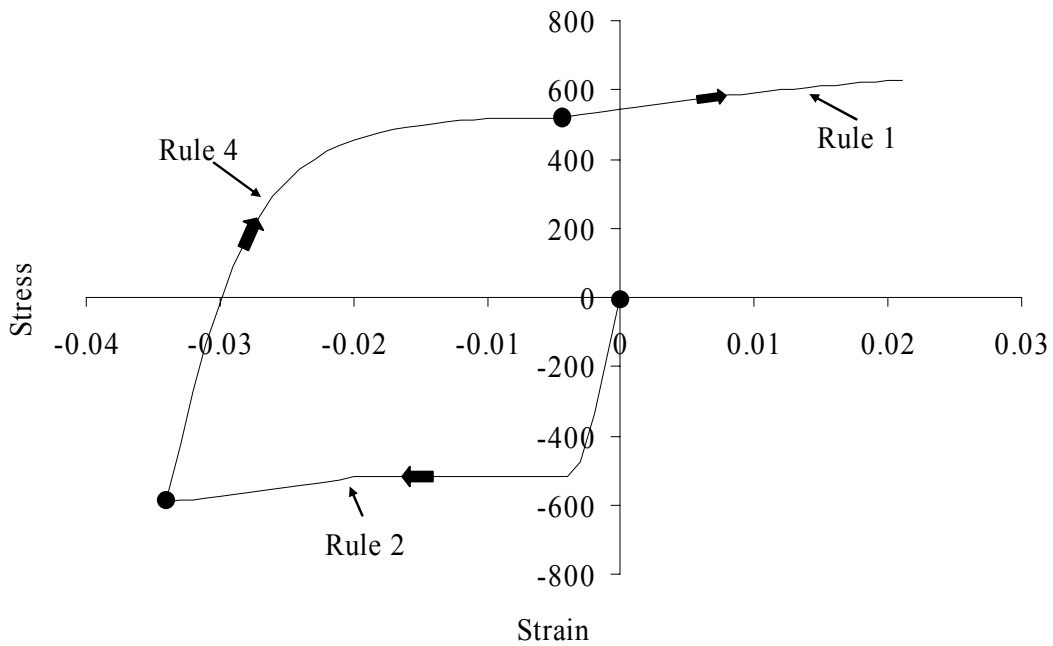

Fig 12 Reversal from rule 2 after strain hardening

Using these parameters the M-P equation can be used to derive the loading reversal curve i.e. the Rule 4. Fig. 12 shows the transition from Rule 2 to Rule 4 obtained from the numerical simulation of the hysteretic model for steel reinforcing bars.

Returning Branches (Rule 5 and Rule 6): After complete unloading occurs on the unloading reversal branch (rule 3), the current branch merges to rule 2 (Fig.9), but if there is partial unloading then loading returning branch (rule 5) is considered, shown in Fig. 13. Similarly, if complete loading occurs on the loading reversal branch (rule 4) then transition from rule 4 to rule 1 takes place (Fig. 11), whereas the partial loading results in generation of unloading returning branch (rule 6), shown in Fig. 13.

Rule 5 (Loading Returning Branch): As described above the reversal from rule 3 will define the starting of rule 5, (Fig. 13). The target strain of rule 5 is given by:

$$\varepsilon_{b5} = \varepsilon_{om}^{+} + \varepsilon_{max} + \Delta\varepsilon_{re}^{+} \tag{115}$$

where:

$$\Delta\varepsilon_{re}^{+} = \varepsilon_{a3} - \varepsilon_{a5} - \frac{f_y^{+}}{1.2E_s} \tag{116}$$

and

$$0 \le \Delta\varepsilon_{re}^{+} \le \frac{f_y^{+}}{3E_s} \tag{117}$$

The target stress f_{b5} and the target slope E_{b5} can be calculated by using equations (100) and (101) respectively. The initial Young's modulus E_{a5} and the M-P parameter R can be calculated from corresponding rule table by putting:

$$\Delta\varepsilon_{a} = \frac{\varepsilon_{b5} - \varepsilon_{a5}}{2} \tag{118}$$

Fig. 13 represents the transition from rule 3 to rule 5 on partial unloading on rule 3. The rule 5 is also summarized in tabular form below.

Parameters	Rule 5

36

$\varepsilon_{sa,5}$	ε_{sr}
$f_{sa,5}$	f_{sr}
$E_{sa,5}$	E_{so}^+
$\varepsilon_{sb,5}$	$\varepsilon_{smax} + \varepsilon_{so}^+ + \varepsilon_{sa3} - \varepsilon_{sa5} - \dfrac{f_{sy}^+}{1.2E_s}$
$f_{sb,5}$	$f_s(\varepsilon_{sb5})$
$E_{sb,5}$	$E_s(\varepsilon_{sb5})$

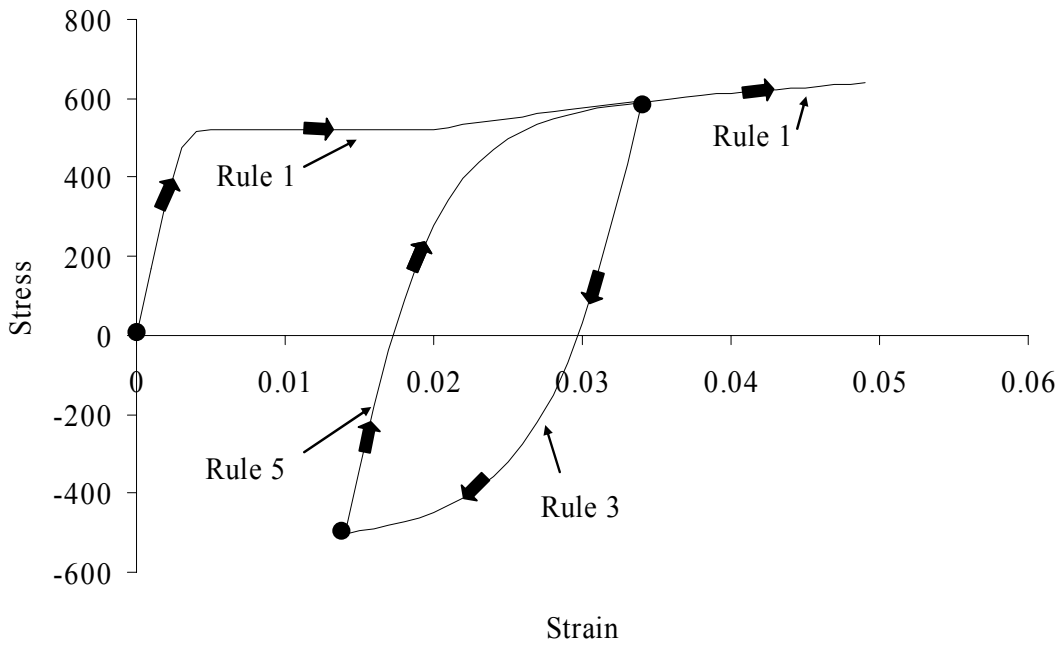The graph is generated from the numerical simulation of hysteretic model for steel reinforcing bars.

Fig 13 Reversal from rule 3

Rule 6 (Unloading Returning Branch): At the occurrence of a reversal on rule 4, rule 6 will start (Fig. 14). The target strain of rule 6 is given by:

37

$$\varepsilon_{sb,6} = \varepsilon_{so}^{-} + \varepsilon_{s\min} + \Delta\varepsilon_{sre}^{-} \tag{119}$$

where:

$$\Delta\varepsilon_{sre}^{-} = \varepsilon_{sa,4} - \varepsilon_{sa,6} - \frac{f_{sy}^{-}}{1.2E_{s}} \tag{120}$$

and

$$0 \geq \Delta\varepsilon_{sre}^{-} \geq \frac{f_{sy}^{-}}{3E_{s}} \tag{121}$$

The target stress $f_{sb,6}$ and the target slope $E_{sb,6}$ can be calculated by using the table described above.

The initial Young's modulus $E_{sa,6}$ and the M-P parameter R_s can be calculated from equation (113) and (114) respectively by putting:

$$\Delta\varepsilon_{sa} = \frac{\varepsilon_{sb,6} - \varepsilon_{sa,6}}{2} \tag{122}$$

Fig. 14 represents the transition from rule 4 to rule 6 on partial loading on rule 4. The graph is generated from the numerical simulation of hysteretic model for steel reinforcing bars.
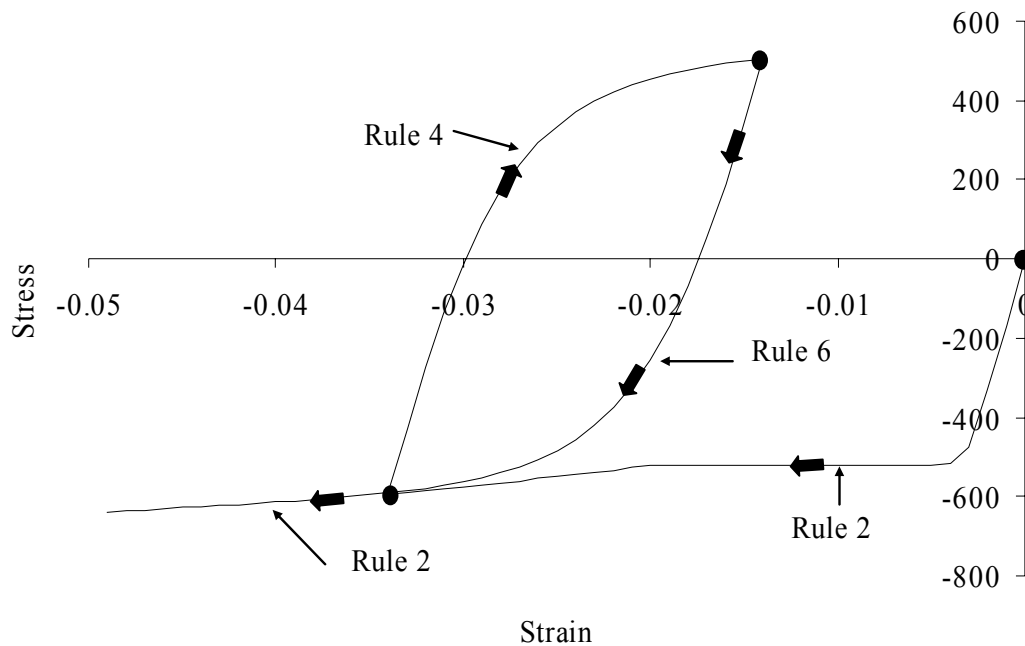
Fig 14 Reversal from rule 4

First Transition Branches (Rule 7 and Rule 8): The curve followed after a reversal from the envelope branch is called as reversal branch, the one followed by a reversal from a reversal branch is called as returning branch. The curve which is obtained after reversal from the returning branch is called as the first transition branch. Partial loading on loading returning branch (rule 5) gives rise to the first transition branch (rule 7), shown in Fig. 15. Similarly, the partial unloading on the unloading returning branch (rule 6) gives rise to the first transition branch (rule 8), shown in Fig. 16.

Rule 7 (First Transition Branch): In case of reversal from rule 5, when partial loading is done on rule 5, rule 7 will follow from that point onwards, rule 7 will target the starting point of rule 5, which is also the reversal from rule 3. The vital parameters are shown in tabular form.

39

Parameters	Rule 7
$\varepsilon_{sa,7}$	ε_{sr}
$f_{sa,7}$	f_{sr}
$E_{sa,7}$	E_{so}^-
$\varepsilon_{sb,4}$	$\varepsilon_{sa,5}$
$f_{sb,4}$	$f_{sa,5}$
$E_{sb,4}$	$E_{sa,3}(\varepsilon_{sa,5})$

where, $E_{sa,3}(\varepsilon_{sa,5})$ is the tangential modulus calculated on rule 3 corresponding to the strain $\varepsilon_{sa,5}$. The Menegotto Pinto equation can then be used to connect these two points.

Fig. 15 represents the generation of rule 7 after reversal from rule 5 in the case of partial loading. This graph is generated from the numerical simulation of hysteretic model for steel reinforcing bars. In the case of complete loading on loading returning branch (rule 5), the transition from rule 5 to rule 1 takes place.
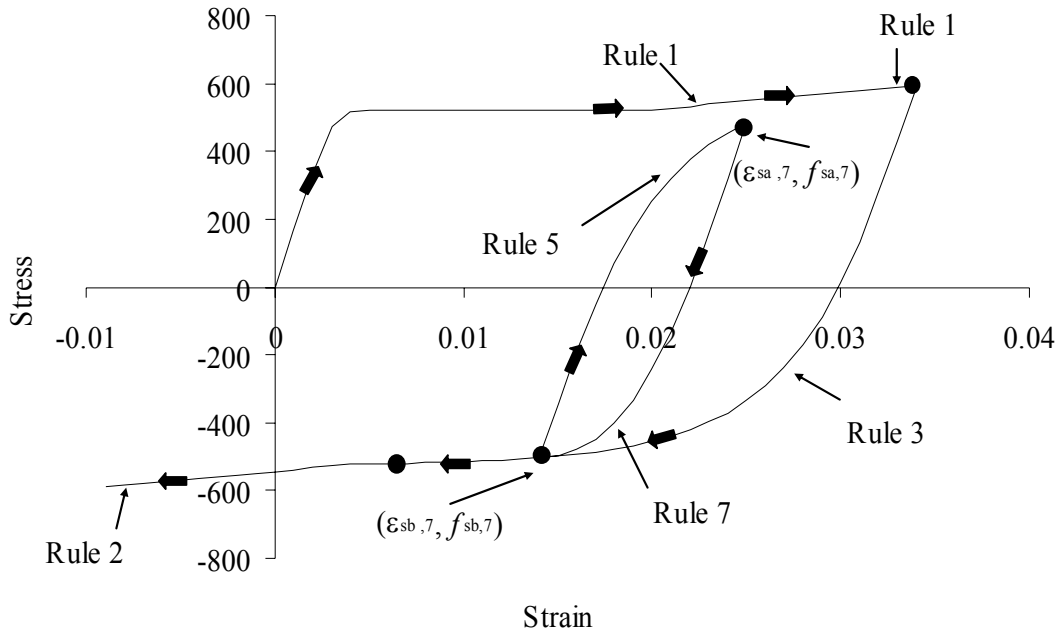
Fig 15 Reversal from rule 5

Rule 8 (First Transition Branch): In case of reversal from rule 6, when partial unloading is done on rule 6, the first transition branch (rule 8) will start from this point, which will target starting of rule 6. The vital parameters are summarized in tabular form below:

Parameters	Rule 8
$\varepsilon_{sa,8}$	ε_{sr}
$f_{sa,8}$	f_{sr}
$E_{sa,8}$	E_{so}^{+}
$\varepsilon_{sb,8}$	ε_{sa6}
$f_{sb,8}$	f_{sa6}
$E_{sb,8}$	$E_{sa,4}(\varepsilon_{sa,6})$

The target stress $f_{sb,8}$ and the target slope $E_{sb,8}$ are calculated from table. Fig. 16 represents the generation of rule 8 after reversal from rule 6 in the case of partial unloading. This graph is generated from the numerical simulation of hysteretic model for steel reinforcing bars.
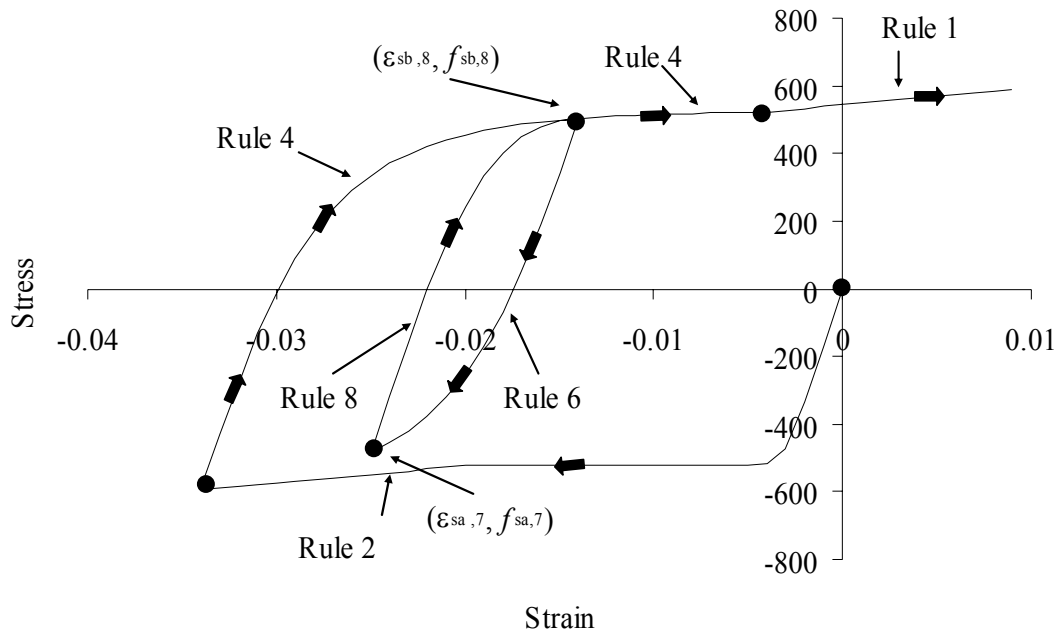

Fig 16 Reversal from rule 6

Second Transition Branches (Rule 9 and Rule 10): Partial unloading on rule 7 gives rise to the second transition branch (rule 9), shown in Fig. 17, whereas the complete unloading on rule 7 results in transition from rule 7 to rule 3 (Fig. 17). Similarly, the partial loading on rule 8 gives rise to the second transition branch (rule 10), shown in Fig.18, whereas the complete loading on rule 8 results in transition from rule 8 to rule 4 (Fig. 18).

Rule 9 (Second Transition Branch): In case of reversal from rule 7, when partial unloading is done on rule 7,rule 9 will follow from that point onwards. The curve that

42

follows a reversal from rule 7 is called as the second transition curve (rule 9) whose target point is defined as:

$$\varepsilon_{sb,9} = \varepsilon_{sa,7} \tag{123}$$

The target stress $f_{sb,9}$ and the target slope $E_{sb,9}$ are calculated on rule 5. Fig. 17 represents the generation of rule 9 after reversal from rule 7 in the case of partial unloading. The vital parameters required for rule 9 are summarized in tabular form below.

Parameters	Rule 8
$\varepsilon_{sa,9}$	ε_{sr}
$f_{sa,9}$	f_{sr}
$E_{sa,9}$	E_{so}^{+}
$\varepsilon_{sb,9}$	ε_{sa7}
$f_{sb,9}$	f_{sa7}
$E_{sb,9}$	$E_{sa,7}(\varepsilon_{sa7})$

This graph is generated from the numerical simulation of hysteretic model for steel reinforcing bars.

Rule 10 (Second Transition Branch): In case of reversal from rule 8, when partial loading is done on rule 8, rule 8 will follow from that point onwards. The curve that follows a reversal from rule 8 is called as the second transition curve (rule 10) whose target point is defined as:

$$\varepsilon_{sb,10} = \varepsilon_{sa,8} \tag{124}$$

The target stress $f_{sb,10}$ and the target slope $E_{sb,10}$ are calculated on the rule 6. Fig.18. represents the generation of rule 10 after reversal from rule 8 in the case of partial loading. This graph is generated from the numerical simulation of hysteretic model for steel reinforcing bars.

The below figure also summarizes a schematic representation of all the possible rules and their combinations. The variables required for the rules are also summarized in the tabular form below.
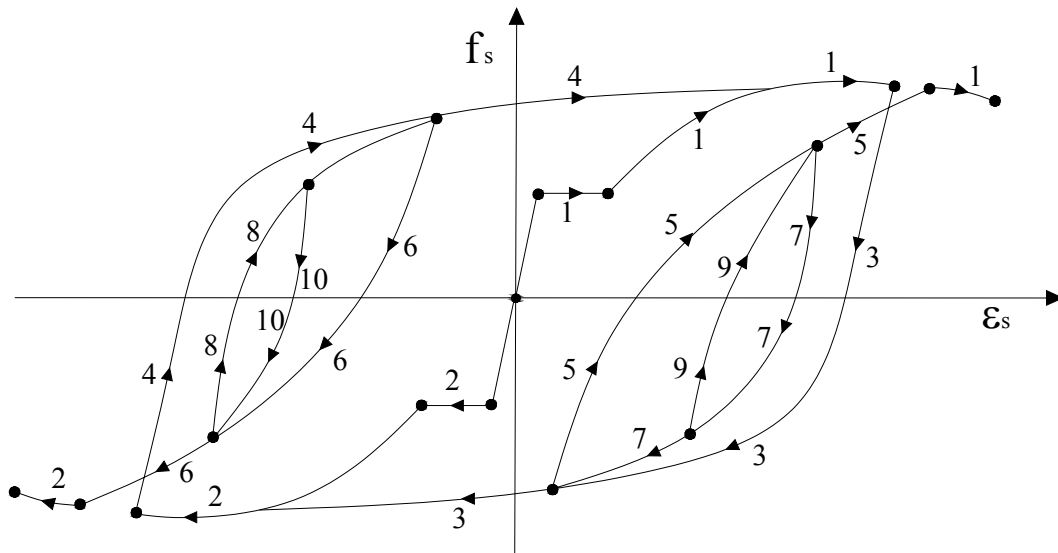

Fig 19 Schematic representation of the constitutive steel laws

Parameter	Rule number							
	3	4	5	6	7	8	9	10
ε_{sai}	ε_{sr}	ε_{sr}	ε_{sr}	ε_{sr}	ε_{sr}	ε_{sr}	ε_{sr}	ε_{sr}
f_{sai}	f_{sr}	f_{sr}	f_{sr}	f_{sr}	f_{sr}	f_{sr}	f_{sr}	f_{sr}

E_{sai}	E_{so}^-	E_{so}^+	E_{so}^+	E_{so}^-	E_{so}^-	E_{so}^+	E_{so}^+	E_{so}^-
ε_{sbi}	$\varepsilon_{smin}+\varepsilon_{so}^-$	$\varepsilon_{smax}+\varepsilon_{so}^+$	$\varepsilon_{smax}+\varepsilon_{so}^+ +\varepsilon_{sa3}-\varepsilon_{sa5} -\dfrac{f_{sy}^+}{1.2E_s}$	$\varepsilon_{smin}+\varepsilon_{so}^- +\varepsilon_{sa4}-\varepsilon_{sa6} -\dfrac{f_{sy}^-}{1.2E_s}$	ε_{sa5}	ε_{sa6}	ε_{sa7}	ε_{sa8}
f_{sbi}	$f_s(\varepsilon_{sb3})$	$f_s(\varepsilon_{sb4})$	$f_s(\varepsilon_{sb5})$	$f_s(\varepsilon_{sb6})$	f_{sa5}	f_{sa6}	f_{sa7}	f_{sa8}
E_{sbi}	$E_s(\varepsilon_{sb3})$	$E_s(\varepsilon_{sb4})$	$E_s(\varepsilon_{sb5})$	$E_s(\varepsilon_{sb6})$	$E_{sa,5}(\varepsilon_{sa5})$	$E_{sa,6}(\varepsilon_{sa6})$	$E_{sa,7}(\varepsilon_{sa7})$	$E_{sa,8}(\varepsilon_{sa8})$

1.3 CFRP laminates

The stress and strain behaviour of CFRP laminates was assumed to be linear. In the femix to simulate the behaviour, they were assumed to as a linear isotropic material. The figure show the behaviour of the CFRP laminates.
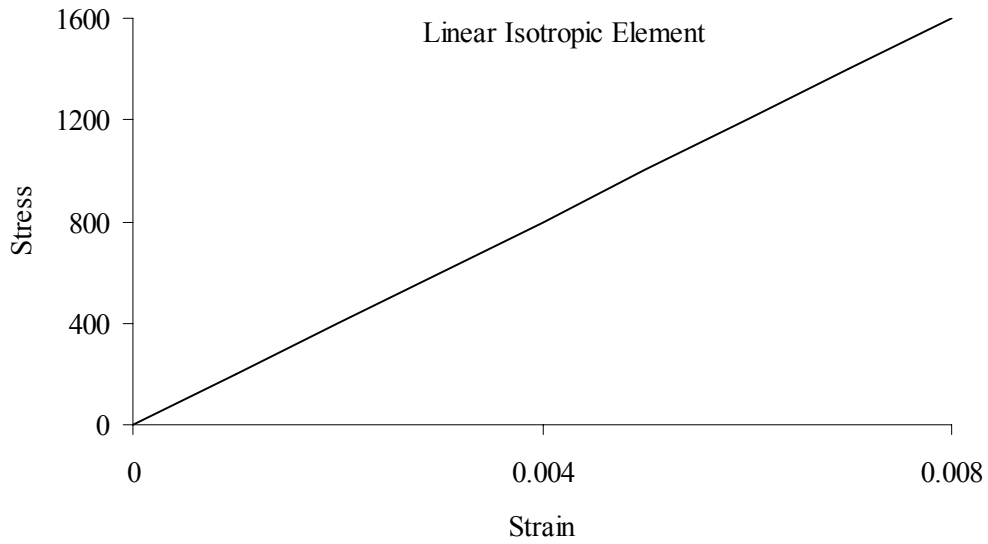

Fig 20 Stress strain relation for linear Isotropic material

2. TIMOSHENKO BEAM THEORY

The current section describes in detail the Timoshenko theory which is applied to each and every fiber element. This theory assumes first-order shear deformation effects in addition to the classical beam theory. In this model CS remain plane and rotate about the neutral axis, but do not remain perpendicular to the deformed longitudinal axis. Transverse shear which remain constant over the cross section accounts for the deviation from perpendicularity of the cross-section with respect to longitudinal axis. The Timoshenko beam theory with finite element formulation is described in detail under the following sections.

2.1 Coordinate Systems

From the analysis and computational point of view, it is not only necessary but important also, to define two coordinate systems, Local and Global coordinate system. The Local coordinate system is used as an intermediate step before the final analysis, which is always performed in Global coordinate system. The relation between the two types of coordinate system is derived later in this section.

2.1.1 Global Coordinate System (GCS)

Global coordinate axis is the only coordinate system which is immobile. For every element its position is fixed, whatever may be the dimension, location and orientation of the element. The GCS axes are represented by g_1, g_2 and g_3, respectively, as shown in Figure 1, which also shows the unit vectors ($\hat{i}_i$) and global displacements (u_i^g and θ_i^g), where $i = 1$, 2 and 3

2.1.2 Local Coordinate System (LCS)

The Local coordinate system is established for each element in order to define the entities related to the element. The LCS is represented by l_1, l_2 and l_3 respectively, with direction of l_1 always tangential to the beam axis (Figure 2).
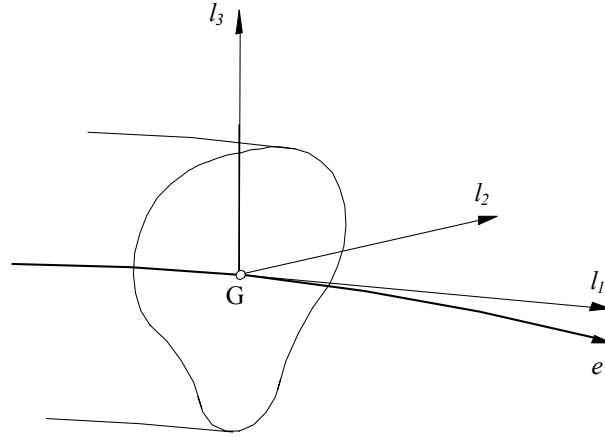
46

Fig 21 Local coordinate system (LCS) of the element

The transformation from one coordinate system to other i.e. from LCS to GCS and vice-versa is derived here. Consider a typical element (Figure 3) randomly located in GCS with the assumed LCS shown, assumed to have natural coordinate (s_1) which stretches from -1 to +1 along the axis. Moreover it is assumed that one of local coordinate axis direction is always concurrent to the axis of the beam; therefore the direction of the tangential axis is derivative of the curvilinear axis. It is to be noted that all the point on the axis of the element can be expressed in terms of curvilinear coordinate system.

The vector l_1 is tangent to the curvilinear axis s_1, so the derivative of the global coordinates with respect to s_1 will generate a vector in direction of l_1. Thus,

$$\underline{l_1} = \left[\frac{\partial x_1}{\partial s_1} \ \frac{\partial x_2}{\partial s_1} \ \frac{\partial x_3}{\partial s_1} \right]^T \tag{125}$$

$$\hat{l}_1 = \frac{\underline{l_1}}{\left\| \underline{l_1} \right\|} = \left[\begin{array}{ccc} l_{11} & l_{12} & l_{13} \end{array} \right]^T \tag{126}$$

The unit vector in the direction of l_2 axis can be determined in the following way. If the direction of $\underline{l_1}$ coincide with $\hat{i}_3$, then unit vector in the direction of l_2 can be assumed as

$$\hat{l}_2 = \hat{i}_2 \tag{127}$$

47

Otherwise it can be derived by cross product of $\hat{i}_3$ with $\hat{l}_1$,

$$\hat{l}_2 = \hat{i}_3 \times \hat{l}_1 \tag{128}$$

In analogous way, $\hat{l}_3$ can be generated by the cross product of above two local axes,

$$\hat{l}_3 = \hat{l}_1 \times \hat{l}_2 \tag{129}$$

These generated vector directions can be used to generate the transformation matrix, to transform the variables from local coordinate system to global coordinate system. If $\hat{l}_2$ and $\hat{l}_3$ are represented by the following components,

$$\hat{l}_2 = \begin{bmatrix} l_{12} & l_{22} & l_{23} \end{bmatrix}^T \tag{130}$$

$$\hat{l}_3 = \begin{bmatrix} l_{13} & l_{23} & l_{33} \end{bmatrix}^T \tag{131}$$

$$\overline{T}^{\mathrm{lg}} = \begin{bmatrix} \hat{l}_1 \\ \hat{l}_2 \\ \hat{l}_3 \end{bmatrix} = \begin{bmatrix} l_{11} & l_{12} & l_{13} \\ l_{21} & l_{22} & l_{23} \\ l_{31} & l_{32} & l_{33} \end{bmatrix} \tag{132}$$

2.2 Displacement Field

Any point on the element can have three translational and three rotational displacements. So the displacement field comprises of six components. The displacement field in the LCS and GCS can be represented by $\underline{U}^l$ and $\underline{U}^g$, respectively, with the following components:

$$\underline{U}^l = \begin{bmatrix} u_1^l & u_2^l & u_3^l & \theta_1^l & \theta_2^l & \theta_3^l \end{bmatrix}^T \tag{133}$$

$$\underline{U}^g = \begin{bmatrix} u_1^g & u_2^g & u_3^g & \theta_1^g & \theta_2^g & \theta_3^g \end{bmatrix}^T \tag{134}$$

The displacement field from LCS to GCS can be transformed by the use of transformation matrix.

$$\underline{U}^l = \underline{T}^{lg}\underline{U}^g$$

<div align="center">(6 × 1)   (6 × 6)(6 × 1)</div>

$$\hspace{10cm}(135)$$

$$\underline{\overline{T}}^{lg} = \begin{bmatrix} \overline{T}^{lg} & 0 \\ 0 & \overline{T}^{lg} \end{bmatrix} \hspace{4cm}(136)$$

The theory derived here considers the feasibility of shear centre do not coincide with the centre of gravity of the CS. Consider that G represents the centre of gravity (origin of the local coordinate system) and C represents the shear centre, with x_{2c}^l and x_{3c}^l as the coordinates in the direction of l_2 and l_3 with respect to centre of gravity. Hence translational displacements of any point in the cross section (in LCS) can be written as (see Figure 4)

$$u_1^l(x_1^l, x_2^l, x_3^l) = u_1^l(x_1^l) + x_3^l\theta_2^l(x_1^l) - x_2^l\theta_3^l(x_1^l) \hspace{2cm}(137)$$

$$u_2^l(x_1^l, x_2^l, x_3^l) = u_2^l(x_1^l) - (x_3^l - x_{3c}^l)\,\theta_1^l(x_1^l) \hspace{2cm}(138)$$

$$u_3^l(x_1^l, x_2^l, x_3^l) = u_3^l(x_1^l) + (x_2^l - x_{2c}^l)\,\theta_1^l(x_1^l) \hspace{2cm}(139)$$
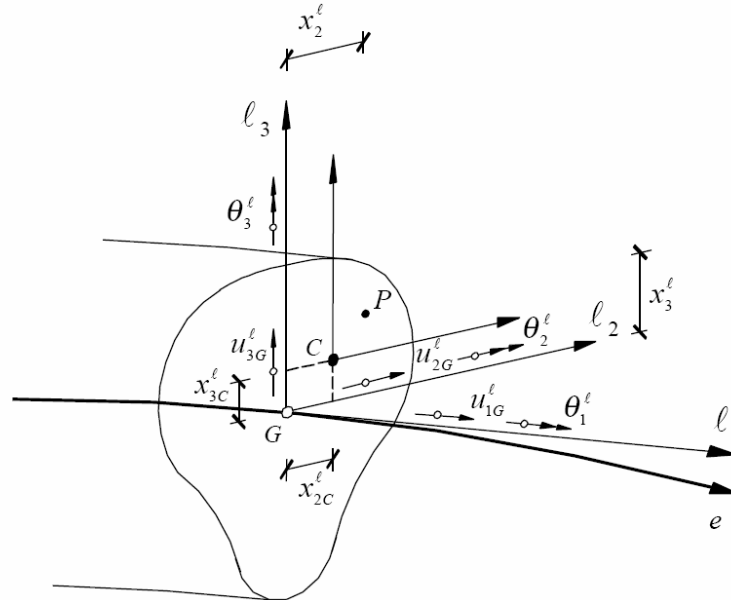

Fig 21 - Generalized displacement field for TB.

49

When shear centre coincides with the centre of gravity the equation 10 reduces to

$$u_1^l(x_1^l, x_2^l, x_3^l) = u_1^l(x_1^l) + x_3^l \theta_2^l(x_1^l) - x_2^l \theta_3^l(x_1^l) \tag{140}$$

$$u_2^l(x_1^l, x_2^l, x_3^l) = u_2^l(x_1^l) - x_3^l \, \theta_1^l(x_1^l) \tag{141}$$

$$u_3^l(x_1^l, x_2^l, x_3^l) = u_3^l(x_1^l) + x_2^l \, \theta_1^l(x_1^l) \tag{142}$$

2.3 Strain components

The strains in the cross section of an element can be calculated using the equations 140-142 in the following way

$$\underline{\varepsilon}^l = \begin{Bmatrix} \varepsilon_1^l \\ \gamma_{12}^l \\ \gamma_{13}^l \end{Bmatrix} = \begin{Bmatrix} \dfrac{\partial u_1^l}{\partial x_1^l} \\[2mm] \dfrac{\partial u_1^l}{\partial x_2^l} + \dfrac{\partial u_2^l}{\partial x_1^l} \\[2mm] \dfrac{\partial u_1^l}{\partial x_3^l} + \dfrac{\partial u_3^l}{\partial x_1^l} \end{Bmatrix} = \begin{Bmatrix} \dfrac{\partial u_1^l}{\partial x_1^l} + x_3^l \dfrac{\partial \theta_2^l}{\partial x_1^l} - x_2^l \dfrac{\partial \theta_3^l}{\partial x_1^l} \\[2mm] -\theta_3^l + \dfrac{\partial u_2^l}{\partial x_1^l} - (x_3^l - x_{3c}^l)\dfrac{\partial \theta_1^l}{\partial x_1^l} \\[2mm] \theta_2^l + \dfrac{\partial u_3^l}{\partial x_1^l} + (x_2^l - x_{2c}^l)\dfrac{\partial \theta_1^l}{\partial x_1^l} \end{Bmatrix} \tag{143}$$

Equations (143) can be transformed in the following format

$$\begin{Bmatrix} \varepsilon_1^l \\ \gamma_{12}^l \\ \gamma_{13}^l \end{Bmatrix} = \begin{bmatrix} 1 & 0 & 0 & 0 & x_3^l & -x_2^l \\ 0 & 1 & 0 & -x_3^l & 0 & 0 \\ 0 & 0 & 1 & x_2^l & 0 & 0 \end{bmatrix} \begin{bmatrix} \dfrac{\partial u_1^l}{\partial x_1^l} \\[2mm] \dfrac{\partial u_2^l}{\partial x_1^l} - \theta_3^l + \theta_{3c}^l \dfrac{\partial \theta_1^l}{\partial x_1^l} \\[2mm] \dfrac{\partial u_3^l}{\partial x_1^l} + \theta_2^l - \theta_{2c}^l \dfrac{\partial \theta_1^l}{\partial x_1^l} \\[2mm] \dfrac{\partial \theta_1^l}{\partial x_1^l} \\[2mm] \dfrac{\partial \theta_2^l}{\partial x_1^l} \\[2mm] \dfrac{\partial \theta_3^l}{\partial x_1^l} \end{bmatrix} \tag{144}$$

or,

$$\begin{Bmatrix} \varepsilon_1^l \\ \gamma_{12}^l \\ \gamma_{13}^l \end{Bmatrix} = \begin{bmatrix} 1 & 0 & 0 & 0 & x_3^l & -x_2^l \\ 0 & 1 & 0 & -x_3^l & 0 & 0 \\ 0 & 0 & 1 & x_2^l & 0 & 0 \end{bmatrix} \begin{bmatrix} \overline{\varepsilon}_a^l \\ \overline{\varepsilon}_s^l \\ \overline{\varepsilon}_t^l \\ \overline{\varepsilon}_b^l \end{bmatrix} = \underline{R}\,\overline{\varepsilon}^l \tag{145}$$

or even

$$\underline{\varepsilon}^l = \underline{R}\,\overline{\underline{\varepsilon}}^l \tag{146}$$

where

$$\overline{\varepsilon}_a^l = \frac{\partial u_1^l}{\partial x_1^l} \tag{147}$$

is the axial strain,

$$\overline{\varepsilon}_s^l = \begin{bmatrix} \dfrac{\partial u_2^l}{\partial x_1^l} - \theta_3^l + \theta_{3c}^l \dfrac{\partial \theta_1^l}{\partial x_1^l} \\ \dfrac{\partial u_3^l}{\partial x_1^l} + \theta_2^l - \theta_{2c}^l \dfrac{\partial \theta_1^l}{\partial x_1^l} \end{bmatrix} \tag{148}$$

are the shear strain components,

$$\overline{\varepsilon}_t^l = \frac{\partial \theta_1^l}{\partial x_1^l} \tag{149}$$

is the torsional strain and

$$\overline{\underline{\varepsilon}}_b^l = \begin{bmatrix} \dfrac{\partial \theta_2^l}{\partial x_1^l} \\ \dfrac{\partial \theta_3^l}{\partial x_1^l} \end{bmatrix} \tag{150}$$

are the flexural strain components.

2.4 Stress and Resultant stresses components

The stress vector in correspondence to the strain vector (eqn. 150) has the following format:

$$\underline{\sigma} = \begin{bmatrix} \sigma_1^l & \tau_{12}^l & \tau_{13}^l \end{bmatrix}^T \tag{151}$$

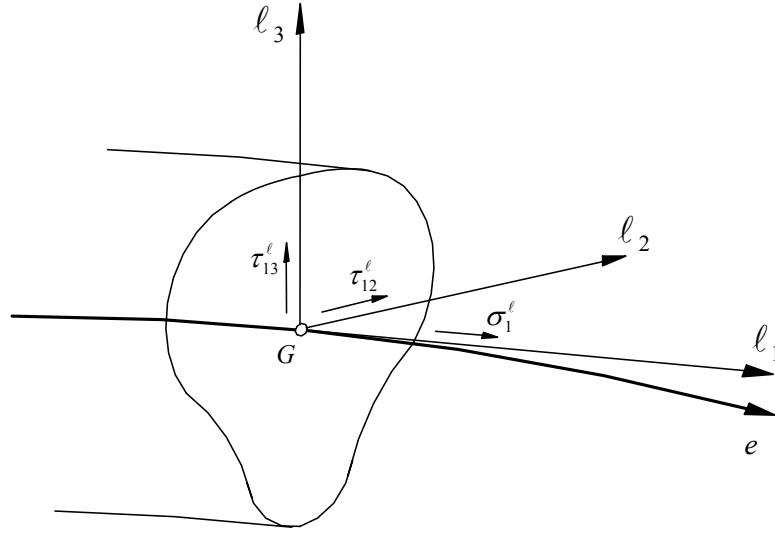whose components are represented in figure 21.

Fig 21 - Stress components

2.4.1 Constitutive equation

Assuming

$$\varepsilon_2^l = \varepsilon_3^l = -\nu\varepsilon_1^l \text{ and } \gamma_{23}^l = 0 \tag{152}$$

The constitutive relation for the 3D Timoshenko beam is

$$\begin{Bmatrix} \sigma_1^l \\ \tau_{12}^l \\ \tau_{13}^l \end{Bmatrix} = \begin{bmatrix} E & 0 & 0 \\ 0 & G & 0 \\ 0 & 0 & G \end{bmatrix} \begin{Bmatrix} \varepsilon_1^l \\ \gamma_{12}^l \\ \gamma_{13}^l \end{Bmatrix} \tag{153}$$

or

$$\underline{\sigma}^l = \underline{D}\,\underline{\varepsilon}^l \tag{154}$$

where E is the longitudinal elasticity modulus of the material and G is the transversal elasticity modulus given by

$$G = \frac{E}{2(1+\nu)} \tag{155}$$

2.4.2 Resultant stresses

Since the 3D Timoshenko Beam has six degrees of freedom at each node, the internal forces are composed of three force and three moment components.

$$\bar{\underline{\sigma}}^l = \begin{bmatrix} N_1^l & V_2^l & V_3^l & M_1^l & M_2^l & M_3^l \end{bmatrix}^T \tag{156}$$

where N_1^l, V_2^l, V_3^l and M_1^l, M_2^l, M_3^l are forces and moments in l_1, l_2 and l_3 directions respectively, which are obtained from the following relationships:

$$N_1^l = \int_A \sigma_1^l dA \tag{157}$$

$$V_2^l = \int_A \tau_{12}^l dA \tag{158}$$

$$V_3^l = \int_A \tau_{13}^l dA \tag{159}$$

$$M_1^l = \int_A (-\tau_{12}^l x_3^l + -\tau_{13}^l x_2^l) dA \tag{160}$$

$$M_2^l = \int_A \sigma_1^l x_3^l dA \tag{161}$$

$$M_3^l = -\int_A \sigma_1^l x_2^l dA \tag{162}$$

where N_1^l is the axial force, V_2^l is the shear force in l_2 direction, V_3^l is the shear force in l_3 direction, M_1^l is the torsion moment, M_2^l is the bending moment in l_2 direction and M_3^l is the bending moment in l_3 direction.

These relations can be arranged in matrix, getting the following format,

$$\bar{\underline{\sigma}}^l = \begin{bmatrix} N_1^l \\ V_2^l \\ V_3^l \\ M_1^l \\ M_2^l \\ M_3^l \end{bmatrix} = \int_A \begin{bmatrix} 1 & 0 & 0 \\ 0 & 1 & 0 \\ 0 & 0 & 1 \\ 0 & -x_3^l & x_2^l \\ x_3^l & 0 & 0 \\ -x_2^l & 0 & 0 \end{bmatrix} \begin{bmatrix} \sigma_1^l \\ \tau_{12}^l \\ \tau_{13}^l \end{bmatrix} dA \tag{163}$$

or

$$\bar{\underline{\sigma}}^l = \int_A \underline{R}^T \underline{\sigma}^l dA \tag{164}$$

Introducing (20b) into (33) and taking into account (13c) results:

$$\bar{\underline{\sigma}}^l = \int_A \underline{R}^T \underline{D} \underline{\varepsilon}^l dA = \int_A \underline{R}^T \underline{D} \underline{R} \bar{\underline{\varepsilon}}^l dA \tag{165}$$

$$\overline{\sigma} = \underline{\hat{D}}\overline{\varepsilon}^l \tag{166}$$

where

$$\underline{\hat{D}} = \int_A \underline{R}^T \underline{D}\underline{R}dA = \int_A \begin{bmatrix} E & 0 & 0 & 0 & x_3^l E & -x_2^l E \\ 0 & G_{12} & 0 & -x_3^l G_{12} & 0 & 0 \\ 0 & 0 & G_{13} & x_2^l G_{13} & 0 & 0 \\ 0 & -x_3^l G_{12} & x_2^l G_{13} & G_{12}(x_3^l)^2 + G_{13}(x_2^l)^2 & 0 & 0 \\ x_3^l E & 0 & 0 & 0 & E(x_3^l)^2 & -x_3^l x_2^l E \\ -x_2^l E & 0 & 0 & 0 & -x_3^l x_2^l E & (x_2^l)^2 E \end{bmatrix} dA \tag{167}$$

Since the material is homogenous, isotropic and moreover with one of the CS principal axis coinciding with the local coordinate axis associated to a given cross section, the following equations should hold,

$$\int_A E x_i^l dA = E \int_A x_i^l dA = 0 \quad (i = 2,3) \tag{168}$$

$$\int_A G x_i^l dA = G \int_A x_i^l dA = 0 \quad (i = 2,3) \tag{169}$$

$$\int_A E x_2^l x_3^l dA = E \int_A x_2^l x_3^l dA = 0 \tag{170}$$

$$\int_A E(x_3^l)^2 dA = E \int_A (x_3^l)^2 dA = EI_2 \tag{171}$$

$$\int_A E(x_2^l)^2 dA = E \int_A (x_2^l)^2 dA = EI_3 \tag{172}$$

$$\int_A [G_{13}(x_2^l)^2 + G_{12}(x_3^l)^2] dA = G \int_A [(x_2^l)^2 + (x_3^l)^2] dA = EI_1 \tag{173}$$

$$\int_A E dA = EA \tag{174}$$

$$\int_A G_{12} dA = \alpha_{12} GA = GA_2^{l*} \tag{175}$$

$$\int_A G_{13} dA = \alpha_{13} GA = GA_3^{l*} \tag{176}$$

where A_2^{l*} and A_3^{l*} are the reduced areas in l_2 and l_3 direction.

therefore, for a section of homogenous and isotropic materials having a CS principal axis coincident with the CS local coordinate system, the resultant stresses are obtained for the following relationship:

$$
\begin{bmatrix} N_1^l \\ V_2^l \\ V_3^l \\ M_1^l \\ M_2^l \\ M_3^l \end{bmatrix} = \begin{bmatrix} EA & 0 & 0 & 0 & 0 & 0 \\ 0 & GA_2^{l*} & 0 & 0 & 0 & 0 \\ 0 & 0 & GA_3^{l*} & 0 & 0 & 0 \\ 0 & 0 & 0 & GI_1^l & 0 & 0 \\ 0 & 0 & 0 & 0 & EI_2^l & 0 \\ 0 & 0 & 0 & 0 & 0 & EI_3^l \end{bmatrix} \begin{bmatrix} \dfrac{\partial u_1^l}{\partial x_1^l} \\[2ex] \dfrac{\partial u_2^l}{\partial x_1^l} - \theta_3^l + \theta_{3c}^l \dfrac{\partial \theta_1^l}{\partial x_1^l} \\[2ex] \dfrac{\partial u_3^l}{\partial x_1^l} + \theta_2^l - \theta_{2c}^l \dfrac{\partial \theta_1^l}{\partial x_1^l} \\[2ex] \dfrac{\partial \theta_1^l}{\partial x_1^l} \\[2ex] \dfrac{\partial \theta_2^l}{\partial x_1^l} \\[2ex] \dfrac{\partial \theta_3^l}{\partial x_1^l} \end{bmatrix} \tag{177}
$$

2.5 Finite Element Formulation

The internal virtual work of a volume V, of a 3D TB element is obtained from the following relation:

$$
\delta W_{\text{int}} = \int_{V^{(e)}} (\delta \varepsilon_1^l \sigma_1^l + \delta \gamma_{12}^l \tau_{12}^l + \delta \gamma_{13}^l \tau_{13}^l) dV^{(e)} \tag{178}
$$

$$
\begin{aligned}
\delta W_{\text{int}} &= \int_{V^{(e)}} \delta(\underline{\varepsilon}^l)^T \underline{\sigma}^l dV \\
&= \int_{V^{(e)}} \delta(\overline{\underline{\varepsilon}}^l)^T \underline{R}^T \underline{D}\underline{\varepsilon}^l dV \\
&= \int_{V^{(e)}} \delta(\overline{\underline{\varepsilon}}^l)^T \underline{R}^T \underline{D}\underline{R}\overline{\underline{\varepsilon}}^l dV \\
&= \int_{L^{(e)}} \delta(\overline{\underline{\varepsilon}}^l)^T (\int_{A^{(e)}} R^T \underline{D}\underline{R} dA) \overline{\underline{\varepsilon}}^l dL \\
&= \int_{L^{(e)}} \delta(\overline{\underline{\varepsilon}}^l)^T \hat{\underline{D}}\overline{\underline{\varepsilon}}^l dL
\end{aligned} \tag{179}
$$

The global coordinates of any point of a finite element can be obtained from the coordinates of the nodes of that element and using the shape functions of the element $N_i(s_1)$. For a n noded finite element, n shape functions will be used to interpolate the coordinates of a generic point at natural coordinate position s_1 :

$$x^g(s_1) = \sum_{i=1}^{n} N_i(s_1)x_i^g \tag{180}$$

where n is the number of nodes per element. For a three noded finite element (180) can have the following format:

$$\begin{bmatrix} x_1^g \\ x_2^g \\ x_3^g \end{bmatrix}(s_1) = \begin{bmatrix} N_1(s_1) & 0 & 0 & ... & N_1(s_1) & 0 & 0 \\ 0 & N_2(s_1) & 0 & ... & 0 & N_2(s_1) & 0 \\ 0 & 0 & N_3(s_1) & ... & 0 & 0 & N_3(s_1) \end{bmatrix} \begin{bmatrix} x_{11}^g \\ x_{21}^g \\ x_{31}^g \\ x_{12}^g \\ x_{22}^g \\ x_{32}^g \\ x_{13}^g \\ x_{23}^g \\ x_{33}^g \end{bmatrix} \tag{181}$$

where x_{ij}^g is the cartesian coordinate of node i in the x_j and $\underline{X}^g$ is the vector of the coordinates in the global reference of the nodes of the finite elements.

$$x^g(s_1) = \begin{bmatrix} \underline{N}_{x_1}(s_1) \\ \underline{N}_{x_2}(s_1) \\ \underline{N}_{x_3}(s_1) \end{bmatrix} \underline{X}^g \tag{182}$$

$$\underline{x}^g(s_1) = \underline{N}_x(s_1)\underline{X}^g \tag{183}$$

2.6 Nodal Displacements

If the nodal displacements are known then the displacements of any point at interior of the element can be calculated using the element shape function in a similar procedure such as the one described in previous section. Adopting an isoparametric formulation, the shape function used for coordinate interpolation can be used for the displacement interpolation. If a finite element of n node is considered, the coordinates of a point at natural coordinate position s_1 is obtained from the following relationship:

$$
\begin{bmatrix} u_1^g \\ u_2^g \\ u_3^g \\ \theta_1^g \\ \theta_2^g \\ \theta_3^g \end{bmatrix}(s_1) =
\begin{bmatrix}
N_1(s_1) & 0 & 0 & 0 & 0 & 0 & \ldots & N_n(s_1) & 0 & 0 & 0 & 0 & 0 \\
0 & N_1(s_1) & 0 & 0 & 0 & 0 & \ldots & 0 & N_n(s_1) & 0 & 0 & 0 & 0 \\
0 & 0 & N_1(s_1) & 0 & 0 & 0 & \ldots & 0 & 0 & N_n(s_1) & 0 & 0 \\
0 & 0 & 0 & N_1(s_1) & 0 & 0 & \ldots & 0 & 0 & 0 & N_n(s_1) & 0 \\
0 & 0 & 0 & 0 & N_1(s_1) & 0 & \ldots & 0 & 0 & 0 & 0 & N_n(s_1) & 0 \\
0 & 0 & 0 & 0 & 0 & N_1(s_1) & \ldots & 0 & 0 & 0 & 0 & 0 & N_n(s_1)
\end{bmatrix}
\begin{bmatrix} u_{11}^g \\ u_{21}^g \\ x_{31}^g \\ \theta_{11}^g \\ \theta_{21}^g \\ \theta_{31}^g \\ \vdots \\ u_{1n}^g \\ u_{2n}^g \\ u_{3n}^g \\ \theta_{1n}^g \\ \theta_{2n}^g \\ \theta_{3n}^g \end{bmatrix}
\tag{184}
$$

where u_{ij}^g and θ_{ij}^g are the displacement and rotation of node i in the x_j and,

$$
\underline{U}_n^{\,g} = \begin{bmatrix} u_{1n}^g & u_{2n}^g & u_{3n}^g & \theta_{1n}^g & \theta_{2n}^g & \theta_{3n}^g \end{bmatrix}^T
\tag{185}
$$

is the vector of the displacement components at nth node number in the global coordinate system.

2.7 Matrices relating strains and displacements

Section 2.3 showed that strains can be obtained deriving the displacement field, therefore the strain components at natural coordinate position s_1 of the vector $\overline{\underline{\varepsilon}}^l$ can be obtained from:

$$
\overline{\underline{\varepsilon}}^l(s_1) = \sum_{i=1}^{n} \overline{B}_k(s_1)\underline{U}_k^l
\tag{186}
$$

Where $\underline{U}_k^{\,l}$ is the displacement vector for kth node (k = 1 to n) in the local coordinate system,

$$
\underline{U}_k^{\,l} = \begin{bmatrix} u_{1k}^l & u_{2k}^l & u_{3k}^l & \theta_{1k}^l & \theta_{2k}^l & \theta_{3k}^l \end{bmatrix}^T
\tag{187}
$$

and the strain-displacement matrix ($\underline{B}_k$) is given by

$$
\underline{B}_k(s_1) =
\begin{bmatrix}
\dfrac{dN_k(s_1)}{dx_1^l} & 0 & 0 & 0 & 0 & 0 \\[2ex]
0 & \dfrac{dN_k(s_1)}{dx_1^l} & 0 & x_{3c}^l \dfrac{dN_k(s_1)}{dx_1^l} & 0 & -N_k(s_1) \\[2ex]
0 & 0 & \dfrac{dN_k(s_1)}{dx_1^l} & -x_{2c}^l \dfrac{dN_k(s_1)}{dx_1^l} & N_k(s_1) & 0 \\[2ex]
0 & 0 & 0 & \dfrac{dN_k(s_1)}{dx_1^l} & 0 & 0 \\[2ex]
0 & 0 & 0 & 0 & \dfrac{dN_k(s_1)}{dx_1^l} & 0 \\[2ex]
0 & 0 & 0 & 0 & 0 & \dfrac{dN_k(s_1)}{dx_1^l}
\end{bmatrix}
\tag{188}
$$

Since the displacements of the nodes of the structure are obtained in the global coordinate system, the displacement of the nodes for each finite element need to be transformed to the local coordinate system of the element:

$$
\begin{aligned}
\bar{\varepsilon}^l(s_1) &= \sum_{k=1}^{n} \underline{B}_k(s_1)\left[\underline{T}^{\lg}(s_1)\right]\underline{U}_k^g \\
&= \sum_{k=1}^{n} \bar{\underline{B}}_k(s_1)\underline{U}_k^g
\end{aligned}
\tag{189}
$$

or

$$
\begin{array}{ccccc}
\bar{\varepsilon}^l(s_1) & = & \underline{B}(s_1) & \hat{\underline{T}}^{\lg} & \underline{U}^g \\
(sc \times 1) & & (sc \times t) & (t \times t) & (t \times 1)
\end{array}
\tag{190}
$$

where $\underline{B}(s_1)$ and $\hat{\underline{T}}^{\lg}$ are extended to the element, $\underline{U}^g$ is the vector of the displacements of the element nodes, sc is the total strain components of the element and t is the total number of degrees of freedom per element.

2.7.1 Calculation of Jacobian

To evaluate $dN_k(s_1)/dx_1^l$ of $\underline{B}_k$ the chain derivative rule is applied:

$$
\frac{dN_k}{dx_1^l} = \frac{dN_1}{ds_1}\frac{ds_1}{dx_1^l}
\tag{191}
$$

$$
\frac{dN_k}{dx_1^l} = \frac{dN_1}{ds_1}\frac{1}{J}
\tag{192}
$$

where J is Jacobian, which is derived in the following section.

Since,

$$
dx_1^l(s_1) = \sqrt{(dx_1^g)^2 + (dx_2^g)^2 + (dx_3^g)^2}
\tag{193}
$$

therefore

$$\frac{dx_1^l}{ds_1} = \sqrt{\left(\frac{dx_1^g}{ds_1}\right)^2 + \left(\frac{dx_2^g}{ds_1}\right)^2 + \left(\frac{dx_3^g}{ds_1}\right)^2} \tag{194}$$

The Jacobian for one dimensional TB element with three nodes is given by:

$$\frac{dx_1^l}{ds_1} = \sum_{k=1}^{n}\left(\left(\frac{dN_k}{ds_1}x_{11}^g\right)^2 + \left(\frac{dN_k}{ds_1}x_{21}^g\right)^2 + \left(\frac{dN_k}{ds_1}x_{31}^g\right)^2\right)^{1/2} \tag{195}$$

$$\frac{dx_1^l}{ds_1} = J \tag{196}$$

2.8 Stiffness matrix
The virtual work can also be written as,

$$\delta W_{int} = \int_L \delta(\underline{\bar{\varepsilon}}^l)^T \hat{\underline{D}}^l \underline{\bar{\varepsilon}}^l dL$$
$$= \int_L \delta\left[\underline{U}^g\right]^T \left[\underline{T}^{lg}\right] \underline{B}^T \hat{\underline{D}}^l \underline{B}\underline{T}^{lg}\underline{U}^g dL \tag{197}$$

Converting the integration for the natural coordinate the expression yields:

$$\delta W_{int} = \delta\left[\underline{U}^g\right]^T \int_{-1}^{+1}\left[\underline{T}^{lg}\right]^T \underline{B}^T \hat{\underline{D}}^l \underline{B}\underline{T}^{lg} J ds_1 \underline{U}^g \tag{198}$$

Hence the stiffness matrix can be written as

$$\underline{K} = \int_{-1}^{+1}\left[\underline{T}^{lg}\right]^T \underline{B}^T \hat{\underline{D}}^l \underline{B}\underline{T}^{lg} J ds_1 \tag{199}$$

By using the Gauss Legendre integration the stiffness coefficient can be derived as

$$\underline{K} = \sum_{p=1}^{N_{s1}}\left(\left[\underline{T}^{lg}\right]^T \underline{B}^T \hat{\underline{D}}^l \underline{B} J \underline{T}^{lg}\right)^{(e)} s_1^p W_p \tag{200}$$

2.9 Equilibrium equations and external loads

In each structure node is regarded as a small connector to which elements are attached, and it is argued that assembly of elements and load terms generate a set of equations stating that each node is in equilibrium. Loads applied to a node come from element deformation, from initial stress in elements, from external loads etc. In general the following loading type can act on a structure

1. Point loads;

59

2. Internal point loads;

3. Loads distributed per unit length of the finite element;

4. Gravity loads;

5. Prescribed loads.

2.10.1 Point loads

When concentrated point loads act directly on the discrete nodes of an element, the loads are directly lumped to the load vector without any changes in the corresponding direction. If the external load acting in GCS at n^{th} node is given by $\underline{Q}_n{}^g$,

$$\underline{Q}_n{}^g = \begin{bmatrix} F_1^g & F_2^g & F_3^g & M_1^g & M_2^g & M_3^g \end{bmatrix}_n^T \tag{201}$$

The $\underline{Q}_n{}^g$ is directly lumped to the global load vector $\underline{Q}^g$ corresponding to its nodal degrees of freedom.

2.10.2 Internal point loads

Consider that a point load is applied in between two nodes which is well defined in global coordinate axes, the point of action is A. The load vector at point A in GCS is shown in figure 5 and given by:
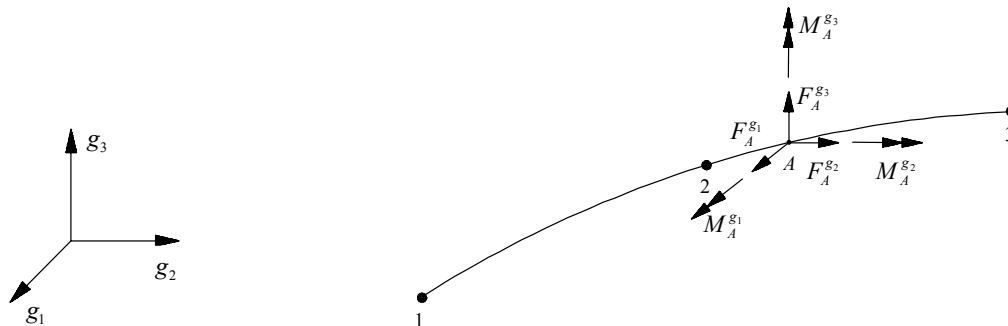

Fig 21 Internal point load in between nodes.

$$\underline{Q}_A^g = \begin{bmatrix} F_1^g & F_2^g & F_3^g & M_1^g & M_2^g & M_3^g \end{bmatrix}_A^T \tag{202}$$

The load vector acting at point A is converted to the equivalent global load vector applied at defined nodal points of the element. By using the virtual work principle the force contribution at any node m can be calculated as:

$$\begin{Bmatrix} F_{1m}^g \delta u_{1m}^g \\ F_{2m}^g \delta u_{2m}^g \\ F_{3m}^g \delta u_{3m}^g \\ M_{1m}^g \delta \theta_{1m}^g \\ M_{2m}^g \delta \theta_{2m}^g \\ M_{3m}^g \delta \theta_{3m}^g \end{Bmatrix} = \begin{Bmatrix} F_{1A}^g \\ F_{2A}^g \\ F_{3A}^g \\ M_{1A}^g \\ M_{2A}^g \\ M_{3A}^g \end{Bmatrix} N_m(s_{1,A}) \begin{Bmatrix} \delta u_{1m}^g \\ \delta u_{2m}^g \\ \delta u_{3m}^g \\ \delta \theta_{1m}^g \\ \delta \theta_{2m}^g \\ \delta \theta_{3m}^g \end{Bmatrix} \tag{203}$$

where

$$\delta U_m^g = \begin{bmatrix} \delta u_{1m}^g & \delta u_{2m}^g & \delta u_{3m}^g & \delta \theta_{1m}^g & \delta \theta_{2m}^g & \delta \theta_{3m}^g \end{bmatrix}^T \tag{204}$$

δU_m^g is virtual displacement vector for node m in the GCS. After canceling the nodal displacements from both sides the equation reduces to

$$\begin{Bmatrix} F_{1m}^g \\ F_{2m}^g \\ F_{3m}^g \\ M_{1m}^g \\ M_{2m}^g \\ M_{3m}^g \end{Bmatrix} = N_m(s_{1,A}) \begin{Bmatrix} F_{1A}^g \\ F_{2A}^g \\ F_{3A}^g \\ M_{1A}^g \\ M_{2A}^g \\ M_{3A}^g \end{Bmatrix} \tag{205}$$

$$\underline{Q}_m^g = N_m(s_{1,A})\underline{Q}_m^g \tag{206}$$

The above method to find the equivalent force at nodes can be compared to the interpolation of the coordinates by using nodal coordinates and shape functions.

2.10.3 Gravity loads

The calculation of the equivalent nodal load vector due to the gravity load vector is derived in this section. It is important that no moments are generated due to such body forces. Consider that the generated loads in the GCS for a small part of element (dV) is given by

$$\begin{Bmatrix} dQ_{V,1}^g \\ dQ_{V,2}^g \\ dQ_{V,3}^g \end{Bmatrix} = \rho \begin{Bmatrix} g_1^g \\ g_2^g \\ g_3^g \end{Bmatrix} dV \tag{207}$$

where g_1^g, g_2^g and g_3^g are accelerations in the direction x_1^g, x_2^g and x_3^g respectively, and ρ is mass per unit volume. By using the virtual work principle, the work done at mth node is given by (in LCS):

$$\left(\underline{F}_V^l \delta \overline{\underline{U}}^l \right)_m = \int_{L^{(e)}} N_m \delta \overline{\underline{U}}_m^l \, \rho \underline{g}^l A dL \tag{208}$$

Converting the accelerations in GCS,

$$\left(\underline{F}_V^l \delta \overline{\underline{U}}^l \right)_m = \int_{L^{(e)}} N_m \delta \overline{\underline{U}}_m^l \overline{\underline{T}}^{lg} \, \rho A \underline{g}^g dL \tag{209}$$

Since both sides include same nodal displacements, so the expression can be reduced to force equation

$$\underline{F}_{V\,m}^l = \int_{L^{(e)}} N_m \overline{\underline{T}}^{lg} \, \rho \underline{g}^g A dL \ . \tag{210}$$

The integration can be performed by Gauss Legendre integral technique and expression reduces to

$$\underline{F}_{V\,m}^l = \sum_{p=1}^{N_{s_1}} \left\{ N_m \underline{F}_V^l J \right\}_{s_1^p} W_p \ . \tag{211}$$

2.10.4 Distributed load applied along the element axis
The possible ways of distribution of forces for a 3D Timoshenko beam is shown in the figure 6. Consider a case of force distribution for any element given by the force vector $\overline{q}_{L,k}^{\ell_j}$ in local coordinate axis with $q = f$ representing force and $q = m$ representing moments. The force equations for a small element dL can be written as –

$$\begin{aligned}
f_L^{\ell_1}(s_1) &= N_1(s_1)\bar{f}_{L,1}^{\ell_1} + N_2(s_1)\bar{f}_{L,2}^{\ell_1} + N_3(s_1)\bar{f}_{L,3}^{\ell_1} \\
f_L^{\ell_2}(s_1) &= N_1(s_1)\bar{f}_{L,1}^{\ell_2} + N_2(s_1)\bar{f}_{L,2}^{\ell_2} + N_3(s_1)\bar{f}_{L,3}^{\ell_2} \\
f_L^{\ell_3}(s_1) &= N_1(s_1)\bar{f}_{L,1}^{\ell_3} + N_2(s_1)\bar{f}_{L,2}^{\ell_3} + N_3(s_1)\bar{f}_{L,3}^{\ell_3} \\
m_L^{\ell_1}(s_1) &= N_1(s_1)\overline{m}_{L,1}^{\ell_1} + N_2(s_1)\overline{m}_{L,2}^{\ell_1} + N_3(s_1)\overline{m}_{L,3}^{\ell_1} \\
m_L^{\ell_2}(s_1) &= N_1(s_1)\overline{m}_{L,1}^{\ell_2} + N_2(s_1)\overline{m}_{L,2}^{\ell_2} + N_3(s_1)\overline{m}_{L,3}^{\ell_2} \\
m_L^{\ell_3}(s_1) &= N_1(s_1)\overline{m}_{L,1}^{\ell_3} + N_2(s_1)\overline{m}_{L,2}^{\ell_3} + N_3(s_1)\overline{m}_{L,3}^{\ell_3}
\end{aligned} \tag{212}$$

In condensed form eqn. (212) can be summarized as

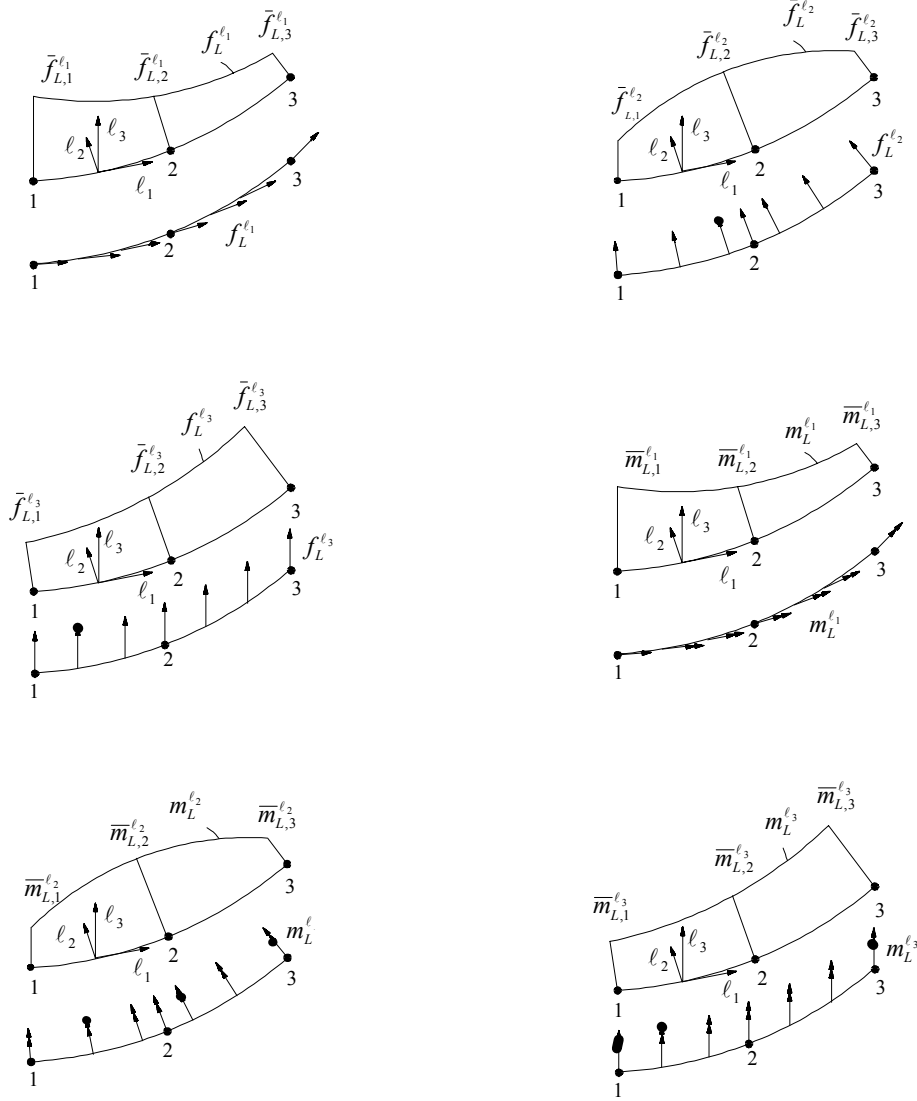$$\underline{q}_L^I(s_1) = \underline{N}(s_1) \left[\underline{q}_L^I \right]^T \tag{213}$$

Fig 6 - Distribution of force on 3D Timoshenko frame element.

where in the condensed equation

$$\underline{\bar{q}}_L^\ell = \begin{bmatrix} \bar{f}_{L,1}^{\ell_1} & \bar{f}_{L,1}^{\ell_2} & \bar{f}_{L,1}^{\ell_3} & \overline{m}_{L,1}^{\ell_1} & \overline{m}_{L,1}^{\ell_2} & \overline{m}_{L,1}^{\ell_3} & \bar{f}_{L,2}^{\ell_1} & \bar{f}_{L,2}^{\ell_2} & \bar{f}_{L,2}^{\ell_3} & \overline{m}_{L,2}^{\ell_1} & \overline{m}_{L,2}^{\ell_2} & \overline{m}_{L,2}^{\ell_3} & \bar{f}_{L,3}^{\ell_1} & \bar{f}_{L,3}^{\ell_2} & \bar{f}_{L,3}^{\ell_3} & \overline{m}_{L,3}^{\ell_1} & \overline{m}_{L,3}^{\ell_2} & \overline{m}_{L,3}^{\ell_3} \end{bmatrix}^T \tag{214}$$

and the shape function matrix is given by

63

$$\underline{N} = \begin{bmatrix} N_1 & 0 & 0 & 0 & 0 & 0 & ... & N_3 & 0 & 0 & 0 & 0 & 0 \\ 0 & N_1 & 0 & 0 & 0 & 0 & ... & 0 & N_3 & 0 & 0 & 0 & 0 \\ 0 & 0 & N_1 & 0 & 0 & 0 & ... & 0 & 0 & N_3 & 0 & 0 & 0 \\ 0 & 0 & 0 & N_1 & 0 & 0 & ... & 0 & 0 & 0 & N_3 & 0 & 0 \\ 0 & 0 & 0 & 0 & N_1 & 0 & ... & 0 & 0 & 0 & 0 & N_3 & 0 \\ 0 & 0 & 0 & 0 & 0 & N_1 & ... & 0 & 0 & 0 & 0 & 0 & N_3 \end{bmatrix} \tag{215}$$

As already mentioned that the equations are derived for a small element, hence they must be integrated over the length to get the equivalent nodal forces. Applying the virtual work principle and integrating the work done:

$$d\underline{Q}_L^{\ell}(s_1) = \underline{q}_L^{\ell}(s_1)\,dL \ . \tag{216}$$

$$\underline{Q}_L^{g}(s_1) = \int\limits_{L^{(e)}} \left[\underline{N}(s_1)\right]^T \underline{q}_L^{g}\,dL \ . \tag{217}$$

The forces should be converted to the GCS by using the following equation of transformation

$$\underline{q}_L^{g}(s_1) = \left[\overline{\underline{T}}^{\ell g}\right]^T \underline{q}_L^{\ell}(s_1) \tag{218}$$

The integration of equation (218) can be performed by Gauss Legendre integration technique.

$$\underline{Q}_L^{g} = \sum_{p=1}^{N_{s_1}} \left\{ \left[\underline{N}\right]^T \left[\underline{T}^{\lg}\right]^T \underline{q}_L^{l} J \right\}_{s_1^p} W_p \tag{219}$$

The generated forces by the equation (219) are represented in the Figure 8 shown below.
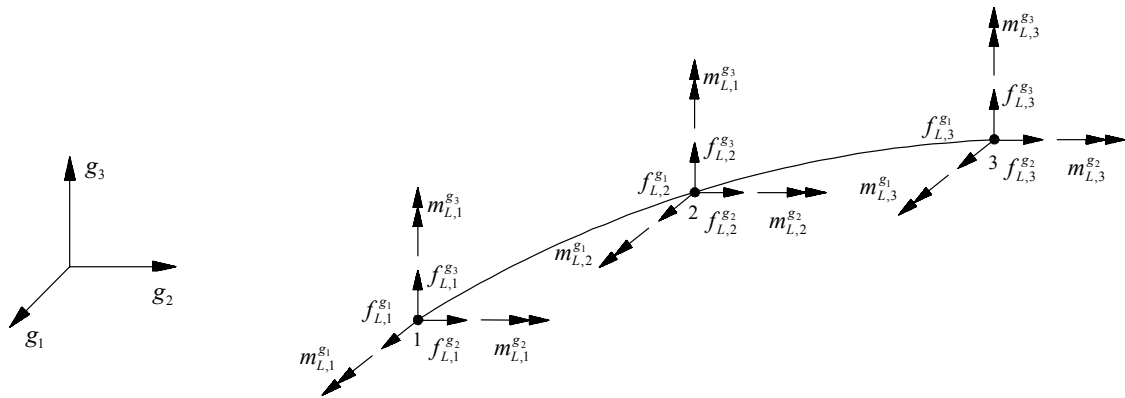

Fig 22 Equivalent force representation at the nodes

3. FIBER MODEL

3.1 Introduction-

A fiber element is designed to model the 3D RC components in the RC structures. Its cross-section can be edited in a divided fibrous form according to the real distribution of steel and concrete in the axial direction. The section during the forced state is assumed to keep a plane, and the average strain and average stress in each cell of the section obey the corresponding constitutive relationship of concrete or steel materials or linear isotropic materials(CFRP laminates). The force and moment acting on the section are obtained by integrating on the section as described in the current section. The section is then reduced to a point on the fiber element, which can be treated as a frame beam element in the analysis of complete structure. Timoshenko Beam theory is used to consider shear deformation which is assumed to be constant in this research, which can also be improved at later stage. The geometrical nonlinear can also be taken into consideration. The Gauss point values are considered in femix for integration of the fibrous element properties. The gauss point refers to the representing point of function for gauss numerical integral. When the element stiffness matrix is formed, the gauss point values with gauss parameters are used instead of the complicated integrating computation. The element internal forces at gauss points can be calculated easily too after global equations are solved.

3.2. Non-linear analysis of Timoshenko frame element

The finite element equilibrium equations derived for static analysis was

$$KU = R \tag{220}$$

The equation correspond to the linear analysis of a structural problem because the displacement (**U**) is a linear function of the applied load vector (**R**); i.e., if the loads are **aR** instead of **R**, where **a** is a constant, the corresponding displacements are **aU**. When this is not the case a *nonlinear* analysis is performed.

Below a computationally efficient method of analysis of reinforced concrete beams and columns is presented. According to this method any element is divided in

65

longitudinal fibers (steel and concrete fibers), and the relation for section force-deformation is derived from stress strain relation of the fibers. The fibers are considered to follow the Timoshenko beam theory presented before. Using fiber, the deformation at their specific locations is calculated and integrated over whole section for the derivation of stiffness matrix. The use of a longitudinal fiber model for the simulation of the non-linear behavior of structures has some advantages. The solution of the system of equations of for non-linear analysis was generated by the application of Newton-Raphson, described later. The algorithm of the implementation of the fibrous model is also described later.

3.3 Stiffness Matrix

The element (e) section is discretized in finite elements (fibers) which follow Timoshenko beam theory, the stiffness matrix for Timoshenko frame element is already derived in section 2.6. The stiffness matrix of every element $K^{(e)}$, is the sum of the stiffness of the fibers (the concrete fibers and steel fibers) of the element. As the stiffness of the element is depending on the stiffness of fibers, the fibers performance depends on the type (steel and concrete) of fiber and the position of fiber w.r.t. neutral axis of element. The stiffness matrixes for steel and concrete fibers are tangent matrix derived from the corresponding non-linear constitutive laws. Moreover the strain in each fiber will be different, so the contribution of stiffness to the element stiffness matrix will also vary. The figure 23 and 24 represents the discretization of frame element in fibrous form.
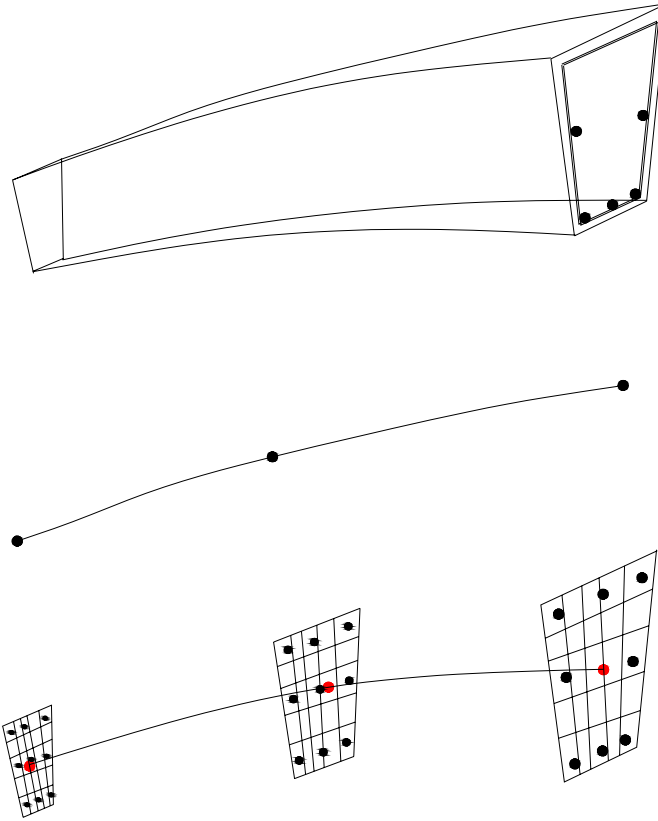
Fig 23 Discretization of an element into longitudinal fibers.

The relation for the incremental stress and incremental strain considered was

$$\Delta\underline{\sigma} \;=\; \underline{D}_T\Delta\underline{\varepsilon} \tag{221}$$

Here $\underline{D}_T$ corresponds to the constitutive tangent stiffness matrix.

The calculation of the stiffness matrix can be summarized in the following steps –

- Evaluation of the generalized displacements (U), at the integration points (Gauss points) for the 3D element,

- Calculation of the deformations ($\underline{\varepsilon}$) at each Gauss points of the finite elements (cells) of the discretized section,

- Calculation of the tangent stiffness matrix ($\underline{D}_T$) at the level of each Gauss point of the section, using the constitutive relations of the material of fiber,

- Calculation of the stiffness matrix for the element (e) (it is sum of the stiffness matrix of all the concrete fibers and steel fibers).
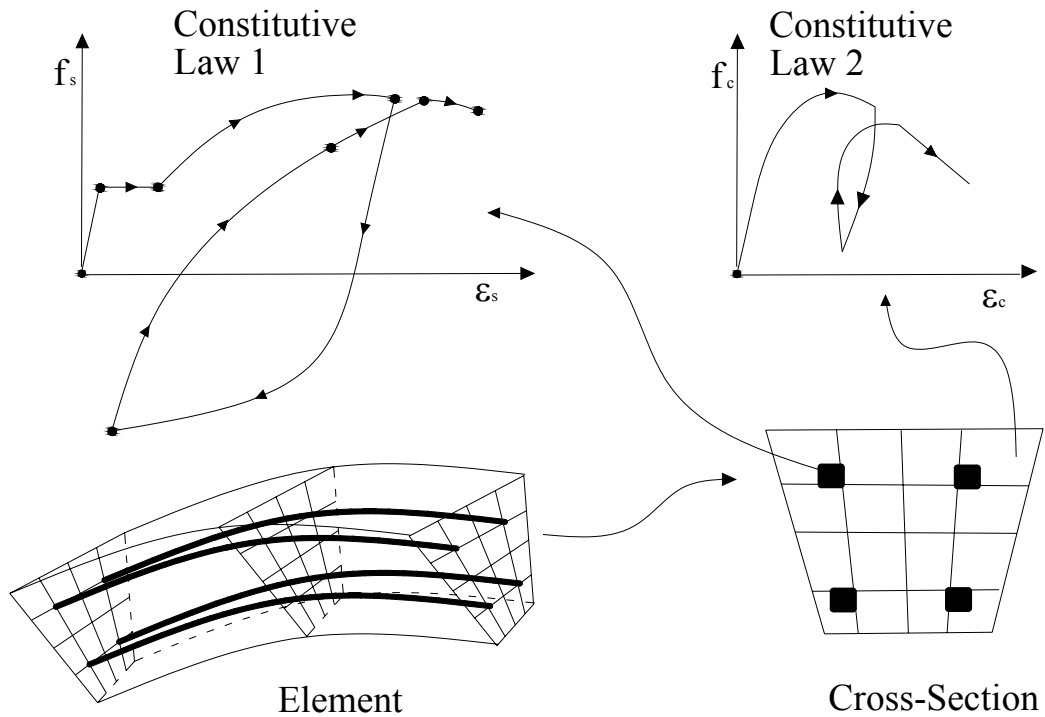
Fig 24 Discretization of an element and fiber behavior.

At the level of each 3D element	$\underline{U}$		$\underline{K}_T$
	$\Downarrow$		$\Uparrow$
At the level of each section	$\underline{\varepsilon}$	$\Rightarrow$	$\underline{\sigma}$

3.3.1 Contribution of the stiffness from the concrete

In the linear analysis the effect of the axial force on the bending moment was neglected and similarly the effect of the shear force on the torsion was also neglected, which can also be seen from the equation derived in the linear analysis of Timoshenko frame element. The equations were derived by the use of virtual work principle for the stiffness

matrix for axial, shear, bending and torsion, but the contribution or the effect of any component on the other was neglected.

For the nonlinear analysis the axial force is considered to have effect on the bending moment and similarly the shear force to have on torsion as shown below

$$\underline{K}_{ab}^{(e)} = \int_{L^{(e)}} \underline{T}_a^{\,\lg} \underline{B}_a^{\,T} \hat{\underline{D}}_{ab} \underline{B}_b \left[\underline{T}_b^{\,\lg} \right]^T dL , \tag{222}$$

$$\underline{K}_{ba}^{(e)} = \int_{L^{(e)}} \underline{T}_b^{\,\lg} \underline{B}_b^{\,T} \hat{\underline{D}}_{ba} \underline{B}_a \left[\underline{T}_a^{\,\lg} \right]^T dL , \tag{223}$$

$$\underline{K}_{st}^{(e)} = \int_{L^{(e)}} \underline{T}_s^{\,\lg} \underline{B}_s^{\,T} \hat{\underline{D}}_{st} \underline{B}_t \left[\underline{T}_t^{\,\lg} \right]^T dL , \tag{224}$$

$$\underline{K}_{ts}^{(e)} = \int_{L^{(e)}} \underline{T}_t^{\,\lg} \underline{B}_t^{\,T} \hat{\underline{D}}_{ts} \underline{B}_s \left[\underline{T}_s^{\,\lg} \right]^T dL . \tag{225}$$

The *subscript*s used above represent

a = parameters related to axial,

b = parameters related to bending,

t = parameters related to torsion and

s = parameters related to shear.

By applying the numerical integration method of Gauss-Legendre, the submatrices of stiffness can be found as shown below –

Sub-matrix associated to the axial deformation –

$$\underline{K}_a^{\,c} = \sum_{p=1}^{N_{s1}^{ab}} \left(\underline{T}_a^{\,\lg} \underline{B}_a^{\,T} \hat{\underline{D}}_a^{\,c} \underline{B}_a \left[\underline{T}_a^{\,\lg} \right]^T J \right)_{s_1^p} W_p \tag{226}$$

$$\hat{\underline{D}}_a^{\,c} = \sum_{i=1}^{NG_{\sec t}} D_{ab,i}^{\,c} A_{GP,i} \tag{227}$$

Where superscript c stands for parameters related to concrete, $NG_{\sec t}$ represents the number of Gauss points in the finite element, A_{GP} the area corresponding to the Gauss point and the longitudinal tangential elasticity at the level of ith Gauss point by $D_{ab,i}^{\,c}$.

Sub-matrix associated to the bending deformation

69

$$\underline{K}_b{}^c = \sum_{p=1}^{N_{s1}^{ab}} \left(\underline{T}_b{}^{\mathrm{lg}} \underline{B}_b{}^T \hat{\underline{D}}_b{}^c \underline{B}_b \left[\underline{T}_b{}^{\mathrm{lg}} \right]^T J \right)_{s_1^p} W_p \tag{228}$$

$$\hat{\underline{D}}_b^c = \begin{bmatrix} \hat{\underline{D}}_{b,11}^c & \hat{\underline{D}}_{b,12}^c \\ \hat{\underline{D}}_{b,21}^c & \hat{\underline{D}}_{b,22}^c \end{bmatrix} = \sum_{i=1}^{NG_{\mathrm{sec}t}} \begin{bmatrix} \hat{\underline{D}}_{ab,i}^c (x_{3,i}^l)^2 A_{GP,i} & -\hat{\underline{D}}_{ab,i}^c x_{2,i}^l x_{3,i}^l A_{GP,i} \\ -\hat{\underline{D}}_{ab,i}^c x_{2,i}^l x_{3,i}^l A_{GP,i} & \hat{\underline{D}}_{ab,i}^c (x_{2,i}^l)^2 A_{GP,i} \end{bmatrix} \tag{229}$$

Where $x_{2,i}^l$ and $x_{3,i}^l$ are the local coordinates of the gauss point of the finite element w.r.t. the centroid of the section of the corresponding finite element.

Sub-matrix associated to the axial-bending interrelation

$$\underline{K}_{ab}{}^c = \sum_{p=1}^{N_{s1}^{ab}} \left(\underline{T}_a{}^{\mathrm{lg}} \underline{B}_a{}^T \hat{\underline{D}}_{ab}{}^c \underline{B}_b \left[\underline{T}_b{}^{\mathrm{lg}} \right]^T J \right)_{s_1^p} W_p \tag{230}$$

$$\hat{\underline{D}}_{ab}^c = \begin{bmatrix} \hat{\underline{D}}_{ab,11}^c & \hat{\underline{D}}_{ab,21}^c \end{bmatrix} = \sum_{i=1}^{NG_{\mathrm{sec}t}} \begin{bmatrix} \hat{\underline{D}}_{ab,i}^c x_{3,i}^l A_{GP,i} & -\hat{\underline{D}}_{ab,i}^c x_{2,i}^l A_{GP,i} \end{bmatrix} \tag{231}$$

Sub-matrix associated to the bending- axial interrelation

$$\underline{K}_{ba}{}^c = \sum_{p=1}^{N_{s1}^{ab}} \left(\underline{T}_b{}^{\mathrm{lg}} \underline{B}_b{}^T \hat{\underline{D}}_{ba}{}^c \underline{B}_a \left[\underline{T}_a{}^{\mathrm{lg}} \right]^T J \right)_{s_1^p} W_p \tag{232}$$

$$\hat{\underline{D}}_{ba}^c = \begin{bmatrix} \hat{\underline{D}}_{ba,11}^c \\ \hat{\underline{D}}_{ba,21}^c \end{bmatrix} = \sum_{i=1}^{NG_{\mathrm{sec}t}} \begin{bmatrix} \hat{\underline{D}}_{ab,i}^c x_{3,i}^l A_{GP,i} \\ -\hat{\underline{D}}_{ab,i}^c x_{2,i}^l A_{GP,i} \end{bmatrix} \tag{233}$$

Sub-matrix associated to the shear deformation

$$\underline{K}_s{}^c = \sum_{p=1}^{N_{s1}^{st}} \left(\underline{T}_s{}^{\mathrm{lg}} \underline{B}_s{}^T \hat{\underline{D}}_s{}^c \underline{B}_s \left[\underline{T}_s{}^{\mathrm{lg}} \right]^T J \right)_{s_1^p} W_p \tag{234}$$

$$\hat{\underline{D}}_s^c = \begin{bmatrix} \hat{\underline{D}}_{s,11}^c & \hat{\underline{D}}_{s,12}^c \\ \hat{\underline{D}}_{s,21}^c & \hat{\underline{D}}_{s,22}^c \end{bmatrix} = \sum_{i=1}^{NG_{\mathrm{sec}t}} \begin{bmatrix} \hat{\underline{D}}_{st,i}^c A_{GP,i}^* & 0 \\ 0 & \hat{\underline{D}}_{st,i}^c A_{GP,i}^* \end{bmatrix} \tag{235}$$

Where $D_{st,i}^c$ is the shear modulus of the concrete.

Sub-matrix associated to the torsional deformation

$$\underline{K}_t{}^c = \sum_{p=1}^{N_{s1}^{st}} \left(\underline{T}_t{}^{\mathrm{lg}} \underline{B}_t{}^T \hat{\underline{D}}_t{}^c \underline{B}_t \left[\underline{T}_t{}^{\mathrm{lg}} \right]^T J \right)_{s_1^p} W_p \tag{236}$$

$$\hat{\underline{D}}_t^c = \sum_{i=1}^{NG_{\text{sect}}} D^c{}_{st,i} \left[(x_{3,i}^l)^2 + (x_{2,i}^l)^2 \right] A_{GP,i} \tag{237}$$

Sub-matrix associated to the shear- torsion interrelation

$$\underline{K}_{st}{}^c = \sum_{p=1}^{N_{s_1}^{st}} \left(\underline{T}_s{}^{\text{lg}} \underline{B}_s{}^T \hat{\underline{D}}_{st}{}^c \underline{B}_t \left[\underline{T}_t{}^{\text{lg}} \right]^T J \right)_{s_1^p} W_p \tag{238}$$

$$\hat{\underline{D}}_{st}^c = \begin{bmatrix} \hat{\underline{D}}_{st,11}^c \\ \hat{\underline{D}}_{st,21}^c \end{bmatrix} = \sum_{i=1}^{NG_{\text{sect}}} \begin{bmatrix} -\hat{\underline{D}}_{st,i}^c x_{3,i}^l A_{GP,i} \\ \hat{\underline{D}}_{st,i}^c x_{2,i}^l A_{GP,i} \end{bmatrix} \tag{239}$$

Sub-matrix associated to the torsion-shear interrelation

$$\underline{K}_{ts}{}^c = \sum_{p=1}^{N_{s_1}^{st}} \left(\underline{T}_t{}^{\text{lg}} \underline{B}_t{}^T \hat{\underline{D}}_{ts}{}^c \underline{B}s_s \left[\underline{T}_s{}^{\text{lg}} \right]^T J \right)_{s_1^p} W_p \tag{240}$$

$$\hat{\underline{D}}_{ts}^c = \begin{bmatrix} \hat{\underline{D}}_{ts,11}^c & \hat{\underline{D}}_{ts,21}^c \end{bmatrix} = \sum_{i=1}^{NG_{\text{sect}}} \begin{bmatrix} -\hat{\underline{D}}_{ts,i}^c x_{3,i}^l A_{GP,i} & \hat{\underline{D}}_{ts,i}^c x_{2,i}^l A_{GP,i} \end{bmatrix} \tag{241}$$

The number of Gauss points of associated to the integration of the sub-matrices of axial, bending, axial-bending and bending-axial are same and equal to $N_{s_1}^{ab}$. Similar is the case for the number of Gauss points associated to the integration of the sub-matrices of shear, torsion, shear-torsion and torsion-shear which is equal to $N_{s_1}^{st}$.

3.3.2 Contribution of the stiffness from the steel

The sub-matrices for the steel are derived below, which are similar to the concrete sub-matrices. The point to be noted is that the number of Gauss point used for calculation of stiffness matrix ($\underline{K}^c$) of concrete should be used for calculation of stiffness matrix ($\underline{K}^s$) steel also.

By knowing the location and the number of the steel fibers, and using the Gauss-Legendre integration technique the sub-matrices can be found in the following manner as described below –

Sub-matrix associated to the axial deformation

$$\underline{K}_a{}^s = \sum_{p=1}^{N_{s1}^{ab}} \left(\underline{T}_a{}^{\lg} \underline{B}_a{}^T \hat{\underline{D}}_a{}^s \underline{B}_a \left[\underline{T}_a{}^{\lg} \right]^T J \right)_{s_1^p} W_p \tag{242}$$

$$\hat{\underline{D}}_a^s = \sum_{i=1}^{NS} D_{ab,n}^s A_{s,n} \tag{243}$$

Where NS is the number of steel fibers in the section, $A_{s,n}$ is the area associated with n[th] steel fiber and $D^s{}_{ab,n}$ is tangential modulus of elasticity for the nth steel fiber.

Sub-matrix associated to the bending deformation

$$\underline{K}_b{}^s = \sum_{p=1}^{N_{s1}^{ab}} \left(\underline{T}_b{}^{\lg} \underline{B}_b{}^T \hat{\underline{D}}_b{}^s \underline{B}_b \left[\underline{T}_b{}^{\lg} \right]^T J \right)_{s_1^p} W_p \tag{244}$$

$$\hat{\underline{D}}_b^s = \begin{bmatrix} \hat{\underline{D}}_{b,11}^s & \hat{\underline{D}}_{b,12}^s \\ \hat{\underline{D}}_{b,21}^s & \hat{\underline{D}}_{b,22}^s \end{bmatrix} = \sum_{i=1}^{NG_{sect}} \begin{bmatrix} \hat{\underline{D}}_{ab,n}^s (x_{3,n}^l)^2 A_{s,n} & -\hat{\underline{D}}_{ab,n}^s x_{2,n}^l x_{3,n}^l A_{s,n} \\ -\hat{\underline{D}}_{ab,n}^s x_{2,n}^l x_{3,i}^l A_{s,n} & \hat{\underline{D}}_{ab,n}^s (x_{2,n}^l)^2 A_{s,n} \end{bmatrix} \tag{245}$$

Where $x_{2,n}^l$ and $x_{3,n}^l$ are the local coordinates of the steel fiber w.r.t. the centre of gravity in l_2 and l_3 direction.

Sub-matrix associated to the axial-bending interrelation

$$\underline{K}_{ab}{}^s = \sum_{p=1}^{N_{s1}^{ab}} \left(\underline{T}_a{}^{\lg} \underline{B}_a{}^T \hat{\underline{D}}_{ab}{}^s \underline{B}_b \left[\underline{T}_b{}^{\lg} \right]^T J \right)_{s_1^p} W_p \tag{246}$$

$$\hat{\underline{D}}_{ab}^s = \begin{bmatrix} \hat{\underline{D}}_{ab,11} & \hat{\underline{D}}_{ab,21} \end{bmatrix} = \sum_{i=1}^{NS} \begin{bmatrix} \hat{\underline{D}}_{ab,n} x_{3,n}^l A_{s,n} & -\hat{\underline{D}}_{ab,n} x_{2,n}^l A_{s,n} \end{bmatrix} \tag{247}$$
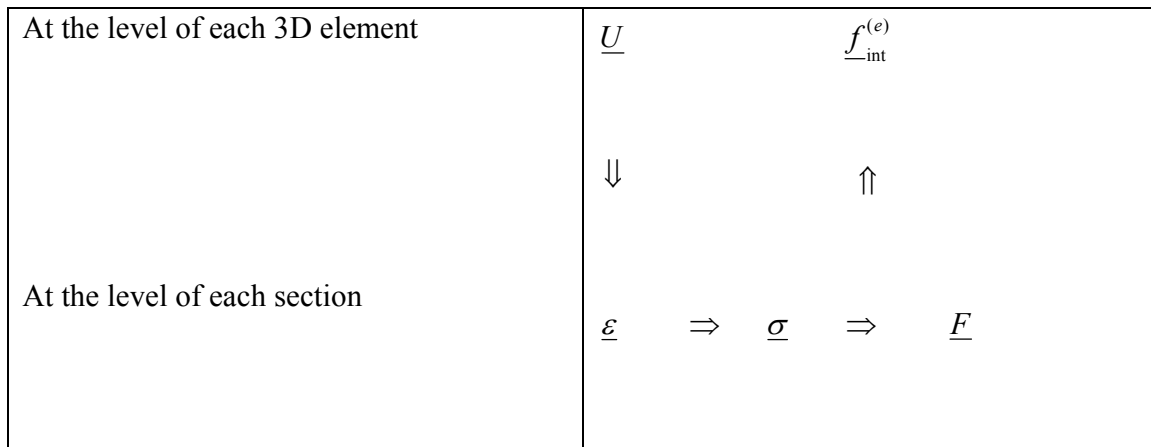
Sub-matrix associated to the bending- axial interrelation

$$\underline{K}_{ba}{}^s = \sum_{p=1}^{N_{s1}^{ab}} \left(\underline{T}_b{}^{\lg} \underline{B}_b{}^T \hat{\underline{D}}_{ba}{}^s \underline{B}_a \left[\underline{T}_a{}^{\lg} \right]^T J \right)_{s_1^p} W_p \tag{248}$$

$$\hat{\underline{D}}_{ba}^s = \begin{bmatrix} \hat{\underline{D}}_{ba,11}^s \\ \hat{\underline{D}}_{ba,21}^s \end{bmatrix} = \sum_{i=1}^{NS} \begin{bmatrix} \hat{\underline{D}}_{ab,n}^s x_{3,n}^l A_{s,n} \\ -\hat{\underline{D}}_{ab,n}^s x_{2,n}^l A_{s,n} \end{bmatrix} \tag{249}$$

3.4 Internal forces

The nodal forces are equivalents to the stresses in the finite elements (fibers) and have to be calculated from the constitutive stress strain relations. The procedure is identical to the calculation of the stiffness matrix. The internal forces in the element ($\underline{f}^{(e)}_{int}$) is the contribution from stresses of steel fibers $\underline{f}^{s}_{int}$ and stresses in the concrete fibers $\underline{f}^{c}_{int}$.

For the calculation of these internal forces in each element, the following procedure can be used effectively –

- Evaluation of the generalized displacements (U), at the integration points (Gauss points) for the 3D element,

- Calculation of the deformations (ε) at each Gauss points of the finite elements (cells) of the discretized section,

- Calculation of the stresses (σ) at the level of each Gauss point of the finite element of section, using the constitutive relations of the material for fiber,

- Integration throughout the section will result in the resultant forces ($\underline{F}$) acting on the section,

- Calculation of the internal forces ($\underline{f}^{(e)}_{int}$) of each 3D element(from stresses of steel fibers $\underline{f}^{s}_{int}$ and stresses in the concrete fibers $\underline{f}^{c}_{int}$).

At the level of each 3D element	$\underline{U}$ $\qquad\qquad\qquad \underline{f}^{(e)}_{int}$
	$\Downarrow \qquad\qquad\qquad \Uparrow$
At the level of each section	$\underline{\varepsilon} \quad \Rightarrow \quad \underline{\sigma} \quad \Rightarrow \quad \underline{F}$

Systemic way for getting the internal forces

3.4.1 Contribution of the Internal forces from the concrete

The contribution of nodal forces from concrete can be calculated by the Gauss-Legendre integration technique by integrating over whole section. The general expressions used are described below –

- Nodal forces corresponding to axial deformation of the finite elements, equivalent to the tension in the element

$$\underline{f}_{\text{int},a}{}^c = \sum_{p=1}^{N_{s1}{}^{ab}} \left(\underline{T}_a{}^{\text{lg}} B_a{}^T N_c J \right)_{s_1^p} W_p \tag{250}$$

$$N_c = \sum_{i=1}^{NG_{\text{sec}t}} \sigma_{ab,i}^c A_{GP,i} \tag{251}$$

Where $\sigma_{ab,i}^c$ is the normal stress in the concrete at the ith Gauss point of the section.

- Nodal forces corresponding to bending deformation of the finite elements, equivalent to bending stresses in the element

$$\underline{f}_{\text{int},b}{}^c = \sum_{p=1}^{N_{s1}{}^{ab}} \left(\underline{T}_b{}^{\text{lg}} B_b{}^T \underline{M}_c J \right)_{s_1^p} W_p \tag{252}$$

$$\underline{M}_c = \sum_{i=1}^{NG_{\text{sec}t}} \left\{ \begin{array}{l} \sigma_{ab,i}^c x_{3,i}^l A_{GP,i} \\ -\sigma_{ab,i}^c x_{2,i}^l A_{GP,i} \end{array} \right\} \tag{253}$$

- Nodal forces corresponding to shear deformation of the finite elements, equivalent to shear stresses in the element

$$\underline{f}_{\text{int},s}{}^c = \sum_{p=1}^{N_{s1}{}^{ab}} \left(\underline{T}_s{}^{\text{lg}} B_s{}^T \underline{Q}_c J \right)_{s_1^p} W_p \tag{254}$$

$$\underline{Q}_c = \sum_{i=1}^{NG_{\text{sec}t}} \left\{ \begin{array}{l} \tau_{12,i}^c A^*{}_{GP,i} \\ \tau_{12,i}^c A^*{}_{GP,i} \end{array} \right\} \tag{255}$$

Where $\tau_{12,i}^c$ and $\tau_{13,i}^c$ are the tangential stress in the concrete at the ith Gauss point of the section in the direction of l_2 and l_3 respectively.

- Nodal forces corresponding to torsional deformation of the finite elements, equivalent to the torsional stresses in the element

$$\underline{f}_{\text{int},t}{}^c = \sum_{p=1}^{N_{s1}{}^{ab}} \left(\underline{T}_t{}^{\text{lg}} B_t{}^T T_c J \right)_{s_1^p} W_p \tag{256}$$

$$T_c = \sum_{i=1}^{NG_{\text{sec}t}} -\tau_{12,i}^c x_{3,i}^l A_{GP,i} + \tau_{13,i}^c x_{2,i}^l A_{GP,i} \tag{257}$$

3.4.2 Contribution of the Internal forces from the Steel

74

The contribution of nodal forces from steel fibers $\underline{f}^{s}_{\text{int}}$ to element ($\underline{f}^{(e)}_{\text{int}}$) can be calculated as described below –

- Nodal forces corresponding to axial deformation of the steel fibers, equivalent to the normal stress in the steel fiber –

$$\underline{f}_{\text{int},a}{}^{s} = \sum_{p=1}^{N_{s1}^{ab}} \left(\underline{T}_{a}{}^{\lg} B_{a}{}^{T} N_{s} J \right)_{s_{1}^{p}} W_{p} \tag{258}$$

$$N_{s} = \sum_{i=1}^{NS} \sigma_{ab,n}^{s} A_{s,n} \tag{259}$$

Where $\sigma_{ab,n}^{s}$ is the normal stress in the nth steel fiber.

- Nodal forces corresponding to bending deformation of the steel fibers, equivalent to bending stresses in the element

$$\underline{f}_{\text{int},b}{}^{s} = \sum_{p=1}^{N_{s1}^{ab}} \left(\underline{T}_{f}{}^{\lg} B_{f}{}^{T} \underline{M}_{s} J \right)_{s_{1}^{p}} W_{p} \tag{260}$$

$$\underline{M}_{s} = \sum_{i=1}^{NS} \left\{ \begin{array}{c} \sigma_{ab,n}^{s} x_{3,n}^{l} A_{s,n} \\ -\sigma_{ab,n}^{s} x_{2,n}^{l} A_{s,n} \end{array} \right\} \tag{261}$$

3.5 Nonlinear Analysis Algorithm – Newton Raphson Method

The response calculation is carried out using a step-by-step increment of load till it reaches the maximum load. The widely used iteration methods in finite element method are based on the classical Newton-Raphson technique. In the present work the method of Newton-Raphson incremental-iterative method is used.

In the non-linear solution algorithm a set of linear matrix relations are iterated till convergence is reached. Theoretically it reaches when the applied loads are perfectly balanced by the internal resisting forces of the elements. Numerically, however, such perfect situation is impossible or computationally very expensive to attain. Hence in such algorithm, it is considered that the convergence is reached when some control parameters, such as unbalanced forces, are smaller than a specified threshold or tolerance. The convergence criteria can be based on the displacement, force or energy.

The decisive factor used here in computational code is of convergence in terms of forces. It is considered that for a kth load increment and i^{th} iteration, the norm of the residual force i.e., the difference between the external forces and the internal forces of this iteration, and norm taken to the exterior forces of this increment; should be lesser than the specified tolerance t.

$$\underline{r}_k^i = \underline{f}_{ext,k} - \underline{f}_{int,k}^{\ i} \tag{262}$$

$$\frac{\left\| \underline{f}_{ext,k} - \underline{f}_{int,k}^{\ i} \right\|}{\left\| \underline{f}_{ext,k} \right\|} < t \tag{263}$$

3.6 Algorithm

Increment of load steps (k= 1 to m)

- If m is the total no of increment in load steps and $\underline{f}_{ext,k}$ represents k^{th} increment of external load value, with $\underline{r}_k^0$ and $\underline{u}_k^0$ representing the initial residual and initial displacement. Applying the Newton-Raphson equation of iteration

$$\underline{f}_{ext,k} = \underline{f}_{ext,k-1} + \underline{\Delta f}_{ext,k} , \tag{264}$$

$$\underline{r}_k^0 = \underline{\Delta f}_{ext,k} + \underline{f}_{k-1}^{final} \tag{265}$$

$$\underline{u}_k^0 = \underline{u}_{k-1}^{final} \tag{266}$$

But for the first iteration when k=1

$$\underline{f}_{ext,k} = 0 ; \underline{r}_k^0 = 0 \text{ and } \underline{u}_k^0 = 0$$

Increment of iterative cycles (i = 1 to n)

- Calculate the stiffness matrix $\underline{K}_{T,k}^i$ with the deformation $\underline{u}_k^{i-1}$, acquired of the previous iteration

- Solve the system of equation

$$\underline{r}_k^{i-1} = \underline{K}_{T,k}^i \underline{\Delta u}_k^i$$

Where $\underline{r}_k^{i-1}$ is the residual of the $(i-1)^{th}$ iteration and k^{th} load increment step.

- Update the nodal displacement

$$u_k^i = u_k^{i-1} + \Delta u_k^i$$

- Calculate the internal nodal force $f_{\text{int},k}^i$ based on the deformations u_k^i

- Calculate the force residual r_k^i

$$r_k^i = f_{ext,k} - f_{\text{int},k}^i$$

- Verify the criteria for the convergence

$$\frac{\left\| f_{ext,k} - f_{\text{int},k}^i \right\|}{\left\| f_{ext,k} \right\|} = \frac{\left\| r_k^i \right\|}{\left\| f_{ext,k} \right\|} < t$$

- If the convergence condition is satisfied then the iteration cycle finishes: with

$$u_k^{final} = u_k^i,$$

$$r_k^{final} = r_k^i$$

and new load increment is done with all the steps described above is followed, if convergence criteria is not met then procedure follows from increment of iterative cycles.

4. APPRAISAL OF MODEL PERFORMANCE

To simulate numerically the tested RC columns, the values included in tables (at the ned of this section) were adopted for the parameters defining the concrete and steel constitutive models. These values were obtained from the data registered in the tests carried out with concrete and steel specimens. A columns was discretized in five elements of three nodes, and two Gauss integration points per element were considered on the evaluation of the stiffness matrix and internal forces. A cross section was discretized in sixteen quadrilateral 4 nodes elements, for the concrete, elements of equal dimensions, with 2×2 Gauss integration points, and four elements to simulate the longitudinal bars. According to the developed approach, at the cross section level any fibre is discretized by a quadrilateral finite element. Due to the rectangular geometry of the simulated RC columns, a four nodded finite elements were used, with an integration scheme of 2×2 Gauss integration points. The cross-section was discretized in sixteen elements the concrete and four elements for the longitudinal steel bars. In case of NSM strengthened RC columns, six additional elements were considered to simulate the CFRP laminates. Following the results obtained in the carried out experimental tests, a linear stress-strain relationship was assumed for the laminates. The values for the parameters that define this relationship were those determined from these tests.

Fig. 24 compares the experimental and numerical envelope curves for tested columns, from which it can be concluded that the developed numerical model captures the mandatory phenomena involved in RC columns submitted to cyclic loading.

78

The capability of the concrete and steel cyclic models, implemented into FEMIX computer program, to simulate the energy dissipated by these materials in the loading cycles can be assessed from the analyses of Fig. 23, which includes the horizontal force-deflection relationship for the columns with 12 mm steel bar diameter. In spite of predicting, with high accuracy, the envelope response, the used cyclic material models estimate for the materials the possibility of dissipating energy larger than that observed in the experimental tests. This is due to the fact that the steel cyclic constitutive model, in the present version, does not contemplate the inelastic buckling phenomenon.

As expected, the laminates had marginal contribution in terms of enhancing the energy absorption capacity for RC columns, since this type of reinforcements can only increase the flexural resistance of the column. The results are shown in figure below-
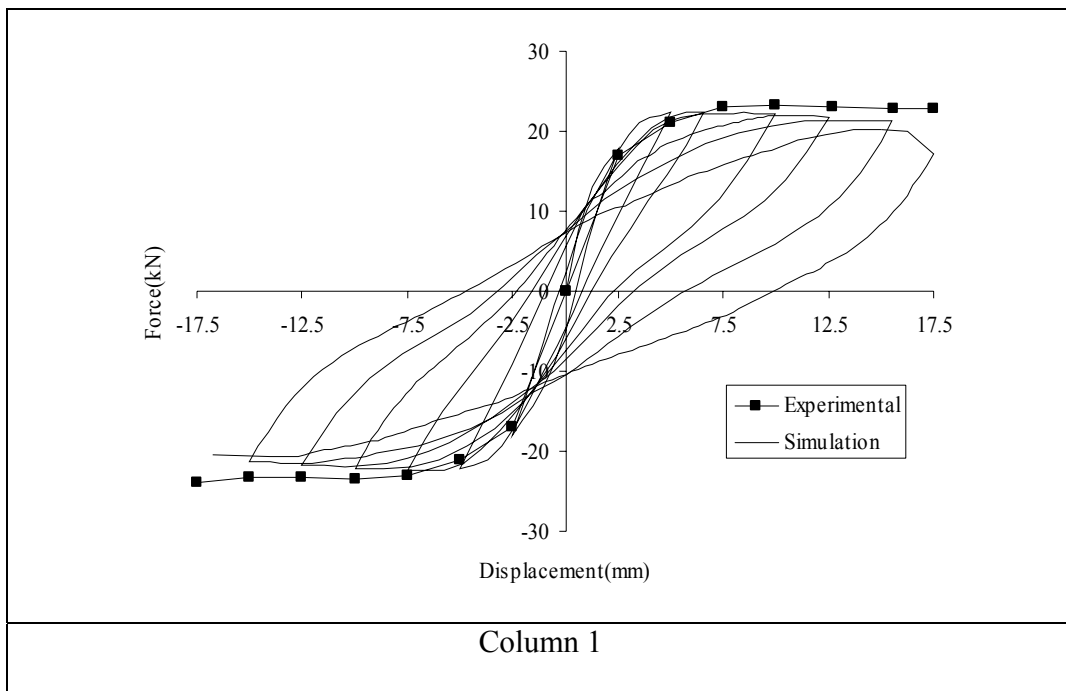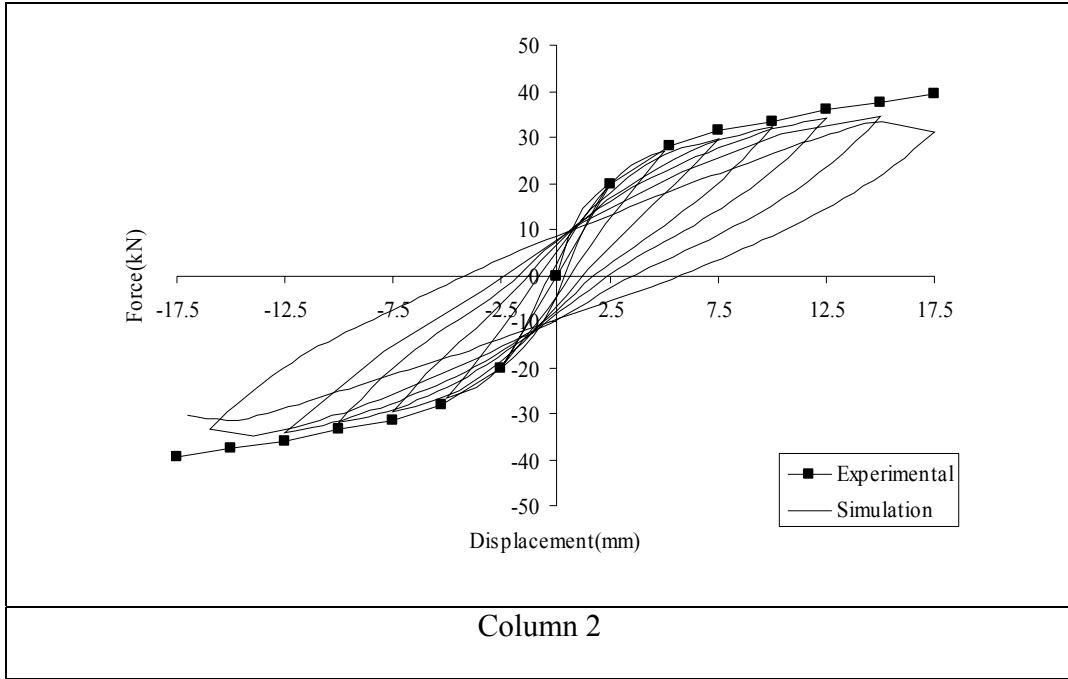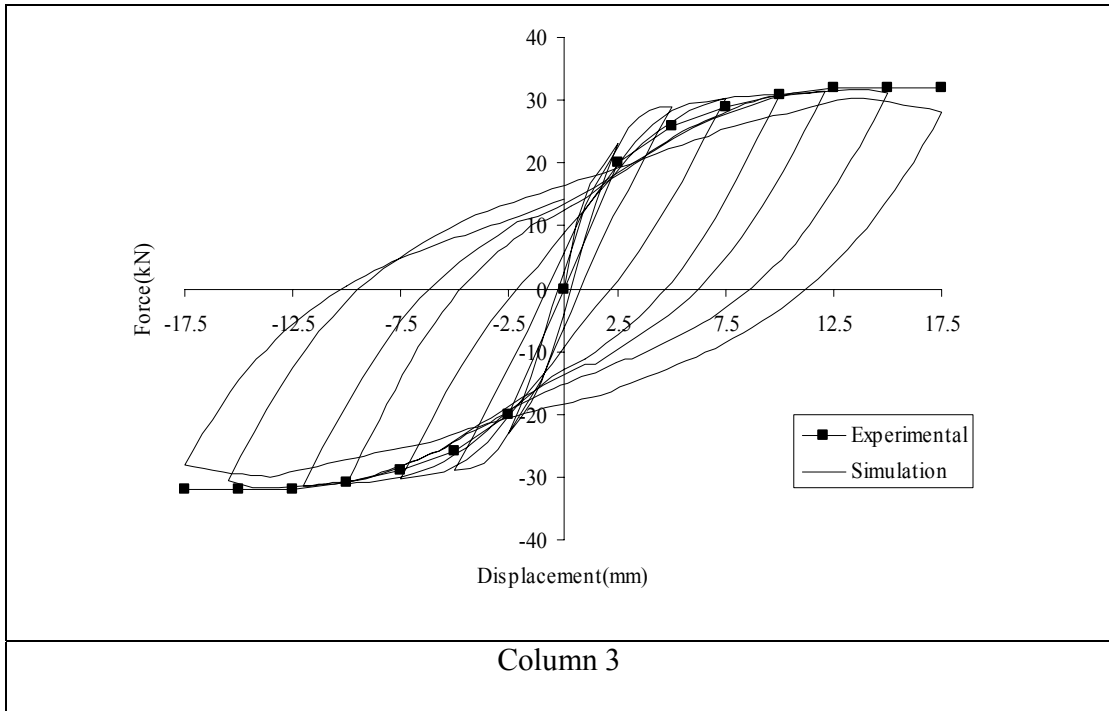

Column 1

Column 2

Fig. 25 Numerical and experimental results on columns 3 and 4
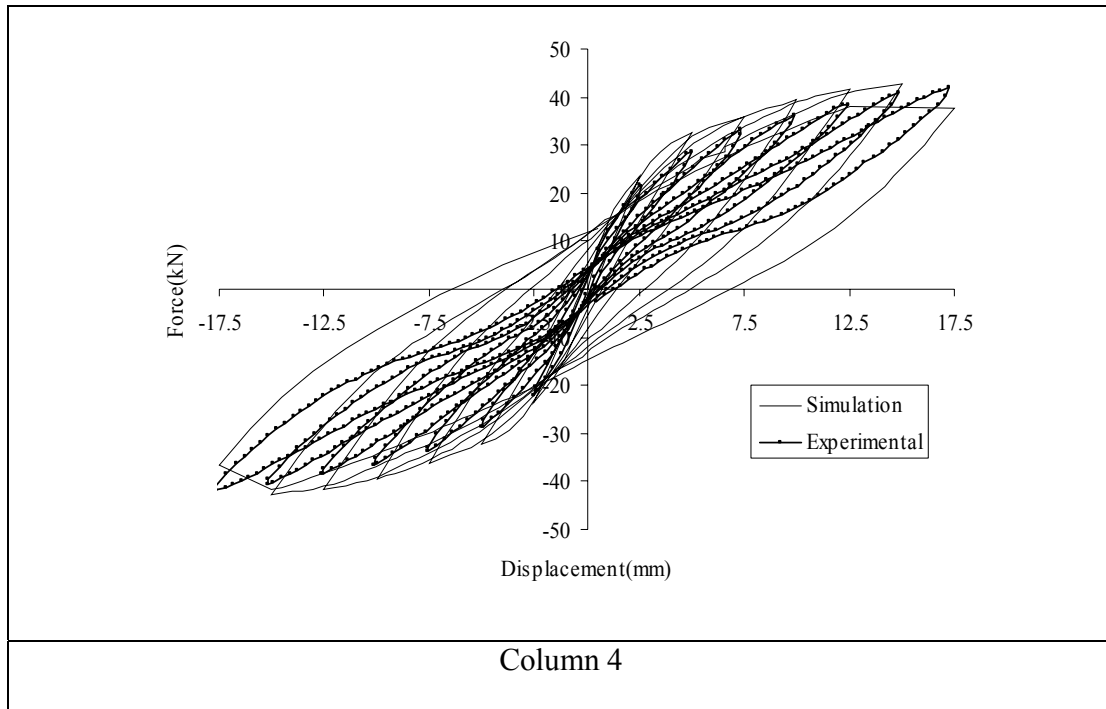

Column 3

Column 4

Fig. 26 Numerical and experimental results on columns 3 and 4

Data used in the numerical analysis to simulate the behaviour of the steel bars.

Column	E_s (N/mm^2)	σ_{sy} (N/mm^2)	ε_{sh}	σ_{sh} (N/mm^2)	ε_{su}	σ_{su} (N/mm^2)	E_{sh} (N/mm^2)
Column 1 and 2	216900	328.0	7.5e-3	344.0	30.0e-3	457.0	6400.0
Column 3 and 4	229700	373.0	3.5e-3	384.0	30.0e-3	519.0	6400.0

Data used in the numerical analysis to simulate the behaviour of the concrete.

Column	f_{cc} (N/mm^2)	ε_{cc}	x_{cr}^-	$E_c^{(1)}$ (N/mm^2)	ε_{ct}	x_{cr}^+	$f_{ct}^{(2)}$ (N/mm^2)
Column 1	13.21	2.50e-3	2	20052	1.20e-4	2	1.20
Column 2	14.79	2.50e-3	2	20821	1.40e-4	2	1.36
Column 3	19.95	2.50e-3	2	23000	2.50e-4	2	1.57
Column 4	17.93	2.50e-3	2	22001	1.89e-4	2	1.42

(1) Uniaxial tensile strength, according to CEB-FIP Model Code (1993)

81

5. CONCLUCIONS

The numerical model can simulate degradation based on the material constitutive laws implemented. The hysteretic behavior of steel is considered vital, as it influences the degrading characteristic of a reinforced concrete. The constitutive laws of steel implemented can simulate the hysteretic behavior of all types of steel. The monotonic behavior of concrete in tension and compression is most efficiently predicted by Tsai, which can describe confined and unconfined behavior rationally The concrete hysteretic behavior can be predicted quite reasonably, for all possible cyclic loading.

This model takes into account the compression non-linear behavior of unconfined and confined concrete, the tensile softening of cracked plain concrete, the tensile stiffening of cracked concrete under the influence of conventional bars and CFRP laminates, the linear shear behavior of concrete, the non-linear behavior of the steel bars and the linear-elastic behavior of CFRP laminates. The behavior of the epoxy mortar, used for repairing the column non-linear hinged region, was simulated by constitutive laws defined from the experimental tests carried out. In the model perfect bond between CFRP laminates and concrete was used, in accordance to the observed test results. This model has reproduced, with good agreement, the behavior registered on the experiments, being a useful tool for analyzing this type of structures.

6. CONCLUCIONS

7. REFERENCE

- Bathe, Klaus-Jurgen (1996). "Finite Element Procedures." Prentice Hall, Inc., USA

- CEB-FIP Model Code 1990 (1993). *Comite Euro-International du Beton*, Bulletin d'Information nº 213/214, Ed. Thomas Telford.

- Chang, G. A. and Mander, J.B. (1994). "Seismic energy based fatigue damage analysis of bridge columns: Part I-Evaluation of seismic capacity", Tech. Report NCEER-94-0006.

- Fillipou, F. C.(1985), "A simple model for reinforcing bar anchorages under cyclic excitations" Earthquake Engineering Research Center, University of California, Berkeley. Gouveia, A. V. (2000). "Análise Experimental e Simulação Numérica de Elementos de Barra de Pórtico Tridimensional de Betão Armado." MSc Thesis, Civil Eng. Dep., University of Minho, Portugal (in Portuguese).

- Guedes, J.P.S.C.M. (1997) "Seismic behaviour of reinforced concrete bridges. Modelling, numerical analysis and experimental assessment", PhD Thesis, Joint Research Centre – ISPRA, Italy.

- Menegotto, M. and Pinto, P. E. (1973). ''Method of analysis for cyclically loaded reinforced concrete plane frames including changes in geometry and non-elastic behavior of elements under combined normal force and bending.'' IABSE Symp. on Resistance and Ultimate Deformability of Struct. Acted on by Well-Defined Repeated Loads, Final Report, Lisbon.

- Reddy J.N. "An Introduction to Finite Element Method." McGraw-Hill, Inc., Singapore.

- Sheshu P. "Textbook of Finite Element Analysis." Prentice Hall of India, Private Limited, New Delhi.

- Taucer, F. F., Spacone, E and Filippou, F. C. (1991) "A fiber beam-column element for seismic response analysis of reinforced concrete structures" Earthquake Engineering Research Center, University of California, Berkeley.

- Timoshenko, S.P., and Gere, James M. "Mechanics of materials. Third edition." PWS-KENT Publishing Company Boston.